Epsins promote atherosclerosis through VSMC phenotypic modulation

Beibei Wang[1]*, Kui Cui[1]*, Bo Zhu[1]*, Yunzhou Dong[1], Donghai Wang[1], Bandana Singh[1], Yao Wei Lu[1], Hao Wu[1], Sudarshan Bhattacharjee[1], Eisa-Beygi Shahram[1], Scott Wong[1], Douglas B. Cowan[1], Mulong Du[2△], Hong Chen[1△]

[1] Vascular Biology Program, Boston Children's Hospital and Department of Surgery, Harvard Medical School, Boston, MA, 02115, USA

[2]Department of Environmental Health, Harvard T.H. Chan School of Public Health, 655 Huntington Avenue, Boston, MA, 02115, USA

△Correspondence to: Hong Chen, PhD, Vascular Biology Program, Boston Children's Hospital and Department of Surgery, Harvard Medical School, Boston, MA, 02115, Email hong.chen@childrens.harvard.edu or Mulong Du, PhD, [2]Department of Environmental Health, Harvard T.H. Chan School of Public Health, 655 Huntington Avenue, Boston, MA, 02115, Email mulongdu@hsph.harvard.edu

* B. Wang, K. Cui, and B. Zhu, contributed equally.

Abstract

Hypothesis: VSMC play crucial roles in atherosclerosis via phenotypic switching. The trans-differentiation of VSMC into other cell types might contribute to atherosclerotic lesion development, progression, and the subsequent diseases such as myocardial infarction or stroke. Epsins, a family of endocytic adaptors, are crucial for atherosclerosis development and progression; yet, the role of epsins in VSMC phenotypic modulation is unknown.

Methods and Results: To decipher the role of VSMC epsins in regulating atheroma development and progression, we created WT and SMC-specific inducible epsin1/2 double knockout (SMC-iDKO) mice on ApoE$^{-/-}$ background fed a western diet. Using single-cell RNA-seq analysis, we found VSMC and EC population significantly changed in SMC-iDKO/ApoE$^{-/-}$ mice compared to ApoE$^{-/-}$ mice. Using immunofluorescent and FACS analysis, we observed that both VSMC and EC marker genes expressions were up-regulated in DKO-VSMCs indicating that DKO-SMCs were maintaining their SMC phenotype and may further trans-differentiating into ECs via a process called MEndoT, mesenchymal to endothelial transition. Given the critical role ofKLF4 in regulating VSMCs phenotype during atheroma progression, we observed diminished KLF4 expression in DKO-SMCs compared to WT treated with oxLDL. Furthermore, we found that epsins interacted with KLF4 with Epsin-UIM domain and their interaction improved KLF4 stability and promoted KLF4 to transfer into nuclei. In this study, we found that epsins were highly expressed and positively correlated with the lesion severity in VSMCs in atherosclerotic. Using immunofluorescent and Oil Red O stainings, we observed reduced lipid accumulation, lesion size and macrophage infiltration but elevated VSMCs in the cap of lesions in SMC-iDKO/ApoE$^{-/-}$ mice compared with ApoE$^{-/-}$ mice.

Conclusions: In conclusions, we demonstrated an unexpected role of epsins in regulating phenotypic switching by repressing SM-contractile and EC marker genes expression through an epigenetic regulatory mechanism. Our data

suggest that epsins may be a therapeutic target for treating occlusive vascular diseases, and uncover regulatory pathways for therapeutic targeting of SMC transitions in atherosclerotic cardiovascular disease.
Key words: atherosclerosis, epsin, phenotypic modulation, vascular smooth muscle cell

Introduction

Atherosclerosis is a chronic inflammatory disease characterized by the progressive accumulation of plaques within arterial walls and the phenotypic plasticity of various cell types, including vascular smooth muscle cells (VSMCs), endothelial cells (ECs), and macrophages[1]. Atherosclerosis may serve as the underlying pathological process for the development and progression of coronary artery disease (CAD)[2]. Among the functional cells, VSMCs are proposed to play central roles in plaque formation, remodeling, and stability during the development and progression of atherosclerosis. Of note, VSMCs undergo “phenotypic switching” that included a process of medial SMC proliferation, dedifferentiation, and migration into the intimal lesions in response to vascular injury[3,4]. Recent SMC-lineage tracing studies in mouse models provided evidence that SMC-derived cells contributed a large proportion of cells within atherosclerotic lesions[5,6]. In addition, population genetic studies have also refocused attention on genes that regulate SMC functions as directly causal role in CAD[7]. However, most current clinical treatments for atherosclerosis target low-density lipoprotein cholesterol and have little direct impact on SMCs per se[8]. Thus, targeting SMCs directly in the context of atherosclerosis holds therapeutic promise, particularly for patients with CAD who exhibit relatively normal cholesterol levels or experience recurrent CAD despite undergoing lipid-lowering therapy.

It is noteworthy that therapeutic interventions, specifically targeting SMC-derived cells involving atherosclerosis, could have both beneficial and detrimental effects, depending on the cellular trajectories and phenotypes. SMC transdifferentiation into “inflammatory” macrophage-like cells might promote instability of atherosclerotic lesions, whereas SMC transition to “synthetic” fibrotic SMCs could stabilize lesions by increasing thickness of the protective fibrous cap[4,9]. A recent study reported that SMCs transdifferentiated predominantly into fibroblast-like cells in atherosclerosis contributing to fibrous cap stability, whereas few SMC-derived macrophage-like cells were detected[10]. Yet this finding argues against several other previous studies of SMC-derived macrophage-like cells in mouse and human lesions[5,6,11,12]. Therefore, it remains uncertain whether VSMC phenotypic switching is predominantly atheroprotective or harmful, or perhaps both, depending on the microenvironment associated with the disease process.

Single-cell RNA sequencing (scRNA-seq) has emerged as a transformative technology for high-resolution cellular heterogeneity and dynamics underlying complex disease pathogenesis[13], which both comprehensively profiles gene

expression patterns within individual cells and enables the identification and characterization of distinct cell populations and transitional states. Through the utilization of scRNA-seq in conjunction with SMC-lineage tracing techniques, a recent study has revealed the notable enrichment of *Vcam1*, a typical EC maker, within SMC-derived intermediate cells in cases of advanced atherosclerosis[14]. However, whether these VSMC-derived cells have endothelial functions, and how they repair or replace the impaired endothelium during atherosclerosis formation have yet to be fully elucidated. Epsins, a family of endocytic adaptors, could play an essential role in the development of atherosclerosis through regulating endothelial-to-mesenchymal transition (EndoMT), lipid uptake and cholesterol efflux, and IP3R1 degradation, evidenced by our previous studies with specific knockout of epsins in ECs and macrophages in mouse models[15-17]. Nevertheless, whether epsins express in VSMC in atherosclerotic plaque and corresponding biological regulation involving cellular interaction and cell transition during arteriosclerosis remains unknown.

Krüppel-like factor 4 (KLF4), a zinc finger transcription factor, played a central role in the phenotypic switching of VSMCs in atherosclerosis through suppressing the expressions of VSMC differentiation marker genes, including *Acta2*, *Tagln*, *Myh11*, and *Cnn1*[5,18], accompanied by a marked reduction in SMC-derived fibroblast-like cells and macrophage-like cells[5]. Moreover, KLF4 has been shown to be subjected to multiple types of posttranslational modifications, including acetylation, methylation, phosphorylation, and ubiquitinoylation[19], such as VHL E3 ligase mediated KLF4 ubiquitylation and thereby promoted its degradation. It is reported that TGF-beta activates the SM α-actin gene expression through promoting KLF4 degradation[20], and KLF4 expression can be suppressed by TGF-beta treatment in VSMCs[21]. Studies suggest that epsins regulate TGF-beta signaling through its effects on receptor endocytosis and downstream signaling pathways[15]. Collectively, we assumed that epsin in VSMCs participated in atherosclerotic plaque pathogenesis through the KLF4 functional pathway.

In this study, we profiled the characteristics of VSMC transition at the single-cell level and explored the cellular interaction underlying epsins-specific loss which would augment VSMC-derived endothelial-like cells, conferring a protective effect against atherosclerotic progression. Functional assessment of VSMC-transdifferentiated endothelial-like cells using Dil-ac-LDL revealed their ability to exhibit the endothelial function, highlighting a potential mechanism for atherosclerosis protection. Furthermore, we demonstrated that epsins preserved KLF4 stability through inhibiting ubiquitinated KLF4 degradation, achieved by direct binding between Epsin1 ENTH+UIM domain and KLF4 within VSMCs. These findings underscored the importance of epsins in the regulation of KLF4 within VSMCs, and potentially open new avenues for therapeutic interventions targeting endothelial repair mechanisms in atherosclerotic pathogenesis.

Method

Primary mouse VSMCs isolation

Mice were anesthetic with isoflurane. Thoracic aortas were isolated from mouse and put in HBSS with penicillin and streptomycin (P/S) at 4°C for 1 hr. Vessels were placed in a sterile culture plate and enzyme solution (Collagenase Type I 5 mg/ml + Collagenase Type IV 5 mg/ml + Liberase Blendzyme 3 0.4 U/ml) was added to cover the vessels. The plates were placed in a 37°C incubator for 2 min. The aortas were transferred to DMEM medium and opened longitudinally with scissors. Remove the adventitia and the endothelial cell layers, then incubated at 37°C in the incubator for about 15 min. After 15 min, cut the aortas into small pieces. Carefully remove the aortic pieces into a 4% gelatin coated 6-well plate, covered with sterile 22 × 22 mm cover slip and add 1 ml complete DMEM medium containing 20% FBS, 1% insulin-transferrin-selenium, 10 ng/ml epidermal growth factor and 1% P/S. Plates were placed in 37°C, 5% CO_2 culture incubator. Feed fresh medium every 3-4 days. As cells grew out and began to cover area (approx. 7 days), flip the cover slips into a new 6-well plate (cell side up) and cover with 2 ml complete DMEM medium. Remove tissue pieces from the plate and refeed cells in original plate. Allow cells to continue to grow until nearly confluent. Cells were weaned into 10% FBS complete DMEM media after passage 3-5 depending on their viability.

siRNA transfection

siRNA transfection was performed according to the manufacture's instructions. Briefly, primary VSMCs were transfected by RNAiMAX (Invitrogen) with scrambled or epsin 1 (UGCUCUUCUCGGCUCAAACUAAGGG) and epsin 2 siRNA duplexes (AAAUCCAACAGCGUAGUCUGCUGUG) designed by Ambion® Silencer® Select Predesigned siRNAs (Invitrogen), or ON-TARGETplus Mouse Pou5f1 siRNA (Invitrogen, CAT#J-046256-05-002). At 48 h post transfection, cells were processed for western blot assays.

Immunofluorescent staining

Human samples: Samples were deparaffinized twice in xylene (15 min for each time), immersed in graded ethanol (100%, 100%, 95%, 90%, 80%, and 70%, each for 3 min), washed in running tap water. After endogenous peroxidase blocking, the samples were blocked in blocking buffer (PBS with 3% donkey serum, 3% BSA and 0.3% Triton X-100), and incubated with primary antibodies anti-αSMA and Epsin1, Epsin2, KLF4 or VHL (1:70 to 1:300 dilution in blocking buffer) at 4°C overnight. Respective secondary antibodies conjugated to fluorescent labels (Alexa Flour 488 or 594; 1:200) were added for 2 hrs at room temperature. The sections were mounted with Fluoroshield™ histology mounting medium with DAPI (1:100).

Mouse samples: Mouse aortic root and BCA cryosections were rewarming at room temperature for 30 min, then fixed by 4% paraformaldehyde for 15 min and blocked in blocking buffer for 1 hr. Sections were then incubated with

primary antibodies anti-αSMA, Epsin1, Epsin2, CD68, CD31, ICAM-1, P-selectin, SM22, Calponin1, Myh11, Cleaved-Caspase3, VE-Cadherin, Galectin3, Ecrg4, KLF4, Oct4 or VHL (1:70 to 1:300 dilution in blocking buffer) at 4°C overnight, followed by incubation with the respective secondary antibodies conjugated to fluorescent labels (Alexa Flour 488, 594 or 647; 1:200) for 2 hrs at room temperature. The sections were mounted with Fluoroshield™ histology mounting medium containing DAPI (1:100).

Cell staining: VSMCs plated on the 18 mm coverslips were washed with PBS for 3 times, fixed with 4% paraformaldehyde for 15 min and blocked with blocking buffer for 1 hr. Coverslips were incubated with primary antibodies anti-αSMA, NRP1, CD31 or VEGFR2; 1:100 to 1:300) at 4°C overnight, followed by incubation with the respective secondary antibodies conjugated to fluorescent labels (Alexa Flour 488 or 594; 1:200) for 1 hr at room temperature. Antibody list, clones and catalogue numbers used for staining are provided in Extended Data Table 1. The sections were mounted with Fluoroshield™ histology mounting medium containing DAPI (1:100). Immunofluorescent images were captured using a Zeiss LSM880 confocal microscope and analyzed with ZEN-Lite 2012 software and HIH ImageJ software.

Atherosclerotic lesion characterization

The whole aortas were collected and fixed with 4% paraformaldehyde. Then, the aortas were stained with Oil Red O for *en face* analysis. Hearts and BCA were embedded in O.C.T and sectioned at 8 microns. Lesion area of the aortic root was quantified by hematoxylin and eosin (H&E) staining. Neutral lipids deposition was determined by Oil Red O staining. Aortic lesion size and lipid content of each animal were obtained by an average of three sections from the same mouse.

***En face* Oil Red O staining**

Whole aortas were dissected symmetrically, pinned to parafilm to allow the *en face* exposed and fixed in formalin for 12 hrs. Aortas were washed in PBS for 3 times, and rinsed in 100% propylene glycol followed by staining with 0.5% Oil Red O solution for 20 minutes at 65°C. Aortas were then put in 85% propylene glycol for 2 minutes, followed by three washes in DD Water. Slides were next incubated with hematoxylin for 30 sec, rinsed in running tap water. Imaging was performed using a Nikon SMZ1500 stereomicroscope, SPOT Insight 2Mp Firewire digital camera, and SPOT Software 5.1.

Oil Red O staining of cryostat sections

Cryostat sections of mouse aortic root and BCA were washed in PBS for 5 mins, then fixed in 4% paraformaldehyde for 15 min. Slices were washed in PBS followed by staining with freshly prepared 0.5% Oil Red O solution in isopropanol for 10 min at 37°C. Slices were then put in 60% isopropanol for 30 sec, followed by 3 washes in water. Slices were next incubated with

hematoxylin for 30 sec, rinsed in running tap water, and mounted with 90% Glycerin.

H&E staining

Cryostat sections of mouse aortic root and BCA were washed in PBS for 5 mins, then fixed in 4% paraformaldehyde for 15 min. Next, slides were stained with 0.1% hematoxylin for 3 min followed by running tap water washes for 10 min. Slices were then dipped in Eosin working solution for 30 sec, quickly rinsed with tap water, dehydrated using graded ethanol (95% and 100% ethanol), followed by transparention by xylene:ethanol absolute (1:1) solution and 100% xylene for 1 hr. Slices were mounted in synthetic resin.

Van Gieson's staining

Van Gieson's staining were performed based on manufacturer's instruction. In brief, Cryostat sections of mouse aortic root and BCA were washed in PBS for 5 mins, then fixed in 4% paraformaldehyde for 15 min. Slices were placed in Elastic Stain Solution (5% hematoxylin + 10% ferric chloride + lugol's lodine Solution) for 20 min, then rinsed in running tap water. Then, slices were dipped in differentiating solution 20 times and in sodium thiosulfate solution for 1 min, following with rinsing in running tap water. Slices were dehydrated in 95% and 100% alcohol once, respectively. Slices were cleared and mounted in synthetic resin.

RNA isolation and quantitative real-time PCR

Total RNA was extracted with RNeasy® Mini Kit based on manufacturer's instruction. cDNA was synthetized by reverse transcription using the iScript cDNA Synthesis Kit (Bio-Rad Laboratories, Inc., Hercules, CA, United States). Quantitative PCR (qPCR) was performed with specific primers using SYBR® Green PCR Master Mix reagent in StepOnePlus Real-Time PCR System. All gene primers can be found in Supplymental Table S2.

Immunoprecipitation and Western Blotting

For immunoprecipitation, VSMCs were lysed with RIPA buffer (50 mM Tris, pH 7.4, with 150 mM NaCl, 1% Nonidet P-40, 0.1% SDS, 0.5% sodium deoxycholic acid, 0.1% sodium dodecyl sulfate, 5 mM N-ethylmaleimide and protease inhibitor cocktail). For KLF4 ubiquitination experiments, VSMCs were lysed using denaturing buffer (1% SDS in 50 mM Tris, pH 7.4) and boiled at 95°C for 10 min to denature protein complexes. Lysates were re-natured using nine volumes of ice-cold RIPA buffer then prepared for immunoprecipitation as follows. Cell lysates were pre-treated with Protein A/G Sepharose beads at 4°C for 2 hrs to remove nonspecific protein followed by centrifugation at 12000 rpm for 5 minutes at 4°C. Supernatant was transferred to a new tube, incubated with Protein A/G Sepharose beads and antibodies against Epsin1 or KLF4 or ubiquitin at 4°C overnight. Mouse IgG was used as negative control. Protein

A/G beads were washed with RIPA buffer for 2 times, followed by PBS for 1 time. Then, beads were suspended with 80 μl 2× loading buffer and heated at 95°C for 10 min. After centrifugation, precipitated proteins were visualized by Western blot. Proteins were resolved by SDS-PAGE gel and electroblotted to nitrocellulose membranes. NC membranes were blocked with 5% milk (w/v) and blotted with antibodies. Western blots were quantified using NIH Image J software.

Differentiation of VSMCs to EC phenotype

EC function was tested with DiI-Ac-LDL Staining Kit based on manufacturer's instruction. Briefly, VSMCs were planted onto 12-mm slides till 95% confluent. and treated with 100 μg/ml oxLDL for 4 days. Then, 10 μg/ml DiI-Ac-LDL (Cell Applications, CAT#022K) was added to instead of oxLDL in the medium onto each 12-mm slide. The slides were placed in a 37°C, 5% CO_2 incubator for 6 hrs. The cells were washed 3 times with wash buffer. The slides were mounted with a cover slip using mounting solution. Images were taken using a Zeiss LSM880 confocal microscope and analyzed with HIH ImageJ software.

Flow cytometry and cell sorting

Prepare a single cell suspension isolated from YFP-VSMC mice aorta. Thoracic aortas were isolated as previous. Aortas were cut into small pieces and moved into a new dish of enzyme solution, incubated at 37°C in the incubator for about 1 hr. After an hour, the plates were washed with 2 ml warmed DMEM medium (DMEM + 5% FBS + P/S). Collect cells by spinning 1500 rpm for 5 min. Carefully remove supernatant and add sterile 0.5 ml PBS containing 1% BSA. Total YFP-tagged VSMCs were sorted as live by using BD FACSARIA II.

Single-cell suspensions used for intracellular staining were fixed, following with 150 μl permeabilization buffer (1% Triton X-100 in PBS) treatment. Add 1 μg blocking IgG and let stand for 15 mins at room temperature. Intracellular cytokines were stained with antibodies to CD31, VE-Cadherin, KLF4 or Oct4 (1:75-1:150). Total YFP-tagged VSMCs were sorted as live, CD31+ or VE-Cadherin+ for KLF4 or Oct4 expression in YFP-VSMC-iDKO/ApoE$^{-/-}$ and YFP-VSMC/ApoE$^{-/-}$ mice. Antibody list, clones and catalogue numbers used for staining are provided in Extended Data Table 1. BD FACSARIA II was used to collect raw data from flow cytometry experiments. All data files were analysed using FlowJo version 9.

Cell culture and plasmids transfection

The HEK 293T cell line (ATCC no. CRL-11268) was used for plasmid transfection to map the binding sites of epsin to KLF4. Flag-tagged Epsin1WT, Epsin1ΔUIM, Epsin1ΔENTH truncation constructs, and pcDNA vector were prepared previously in our lab. pCX4-KLF4 (Plasmid #36118) were purchased

from AddGene. HEK 293T cells were cultured in DMEM (10% FBS and 1% Pen-Strep) at 37°C in humidified air containing 5% CO_2 atmosphere and transfected using Lipofectamine 2000 as instructed by the manufacturer.

Single-cell preparation and Data Processing

Single cell of mouse arterial specimens was prepared as above. The cell viability exceeded 90% determined under the microscope with trypan blue staining. 20 μl of cell suspension was calculated to contain ~20,000 cells for each sample. Single-cell capturing and library construction were performed using the Chromium Next GEM Single Cell 3' Reagent Kits v3.1 (10× Genomics) according to the manufacturer's instructions. In brief, 40 μl of barcoded gel beads, partitioning oil and cell suspension were loaded onto the Chromium Next GEM Chip G to generate single-cell gel beads-in-emulsion. Captured cells were lysed and the transcripts were reverse-transcribed inside individual gel beads-in-emulsion. Full-length cDNA along with cell barcodes were amplified via PCR. The sequencing libraries were constructed by using the 3' Library Kits. Each sample was processed independently. The constructed libraries were sequenced on an Illumina NovaSeq platform.

As similar to our previous study[15], raw sequencing data of FASTQ files were processed using CellRanger (version 3.0.2, 10X Genomics) with default parameters and mapped to mouse reference genome mm10, as well as annotated via a Ensembl 93 annotation, to generate matrices of gene counts by cell barcodes. We used *Seurat* package[22] to conduct quality controls and downstream analyses. For quality controls, genes expressed in less than 10 cells and cells with less than 100 genes were initially removed from the datasets. The subsequent filters at the cell level met the following criteria of number of genes detected per cell > 250, number of UMIs per cell > 500, log10 transformed number of genes detected per UMI > 0.8, and mitochondrial counts ratio < 0.2. Raw unique molecular identifier (UMI) counts were normalized and regressed by mitochondrial mapping percentage using *SCTransform* function. Possible batch effects derived from different conditions on mouse models were adjusted using *Harmony* package[23]. Dimension reduction was performed using principal-component analysis (PCA) with *RunPCA* function. Two-dimensional Uniform Manifold Approximation and Projection (UMAP) was used for visualization. Graph-based clustering was performed on the integrated dataset with a default method of K-nearest neighbor (KNN) graph. Cell clusters were identified using the graph observed above with a resolution parameter ranging from 0.1 to 1.2. In this study, we divided cells into 26 clusters underlying the resolution parameter of 0.8, which were further grouped into 10 cell subgroups.

Trajectory analysis

To calculate the RNA velocity of the single cells, we used the CellRanger output BAM file and GENCODE file to together with the velocyto[24] CLI v.0.17.17 to generate a loom file containing the quantification of spliced and unspliced RNA.

Next, we built a manifold, cluster the cells and visualize the RNA velocities using *scVelo*[25]. cytoTRACE analysis with default parameter[26] was performed to predict differentiation states from scRNA-seq data based on the simple yet robust observation that transcriptional diversity decreases during differentiation, to complement the trajectory analysis from RNA velocity. Pseudotime was analyzed using *Monocle* package[27] with reduceDimension and plot_cell_trajectory functions

Cellular interactions among different cell types

To describe potential cell-to-cell communications, we leveraged the *CellChat* R package[28] to infer the cellular interactions based on the normalized scRNA-seq dataset. The algorithm of CellChat could examine the ligandreceptor interactions significance among different types of cells based on the expression of soluble agonist, soluble antagonist, and stimulatory and inhibitory membrane-bound co-receptors. By summing the probabilities of the ligand-receptor interactions among a given signaling pathway, we could calculate the communication probability for the pathway. In brief, we followed the official workflow and loaded the normalized counts into CellChat and applied the preprocessing functions *identifyOverExpressedGenes*, *identifyOverExpressedInteractions* and *projectData* with standard parameters set. As database we selected the 'Secreted Signaling' pathways and used the pre-compiled 'Protein-Protein-Interactions' as a priori network information. For the main analyses the core functions *computeCommunProb*, *computeCommunProbPathway* and *aggregateNet* were applied using standard parameters and fixed randomization seeds. Finally, to determine the senders and receivers in the network the function *netAnalysis_signalingRole* was applied on the 'netP' data slot.

Gene-based genetic association analysis

We used the publicly available GWAS summary statistics of coronary artery disease (CAD) in European populations[29] from a meta-analysis of three datasets, including UK Biobank SOFT CAD GWAS, the CARDIoGRAMplusC4D 1000 Genomes-based GWAS[30], and the Myocardial Infarction Genetics and CARDIoGRAM Exome[31]. The SOFT CAD phenotype in UK Biobank[29] encompasses individuals with fatal or nonfatal myocardial infarction (MI), percutaneous transluminal coronary angioplasty (PTCA) or coronary artery bypass grafting (CABG), chronic ischemic heart disease (IHD) and angina. CARDIoGRAMplusC4D 1000 Genomes-based GWAS[30] is a meta-analysis of GWAS studies of mainly European, South Asian, and East Asian, involving 60,801 CAD cases and 123,504 controls. Myocardial Infarction Genetics and CARDIoGRAM Exome[31] is a meta-analysis of Exome-chip studies of European descent involving 42,335 patients and 78,240 controls.

A total of 8,908,875 SNPs without exome chip data were retained. We extracted SNPs available in individuals of Utah residents (CEPH) with Northern

and Western European ancestry from 1000 Genomes Project (Phase I, version 3), and then performed quality control using the following criteria: minor allele frequency (MAF) > 0.01, call rate ⩾ 95% and *P* value of Hardy-Weinberg equilibrium (HWE) > 0.01. Eventually, a total of 7,580,209 SNPs were included for further gene analysis. After variant annotation, SNPs were mapped into 17,910 protein-coding genes including the body of the gene or its extended regions (± 20 kb downstream or upstream). The SNP-based *P* values from the GWAS meta-analysis were used as input for the gene-based analysis computed by leveraging a multivariant converging regression model in the Multi-marker Analysis of GenoMic Annotation (MAGMA)[32]. Stringent Bonferroni correction was applied for multiple testing with the genome-wide significance at *P* = 2.79E-6 (0.05/17,910), which generated 68 candidate CAD susceptibility genes for further signature score analysis.

Mendelian Randomization

Summary-level statistics of aptamer-based plasma protein KLF4 were extracted from a large-scale protein quantitative trait loci (pQTL) study in 35,559 Icelanders at deCODE. The levels of protein were rank-inverse normal transformed and adjusted for age and sex. Details on the GWAS can be found in the original publication[33]]. Mendelian Randomization (MR) is an analytical method, which uses genetic variants as instrumental variables (IVs) to assess the causal effect of specific phenotypes on outcomes[34]. We performed two-sample MR analysis to obtain causal estimates of plasma protein KLF4 on CAD using the *TwoSampleMR* package[35]. Independent SNPs (LD r^2<0.001, within 10,000 kb) at *P* < 5e-8 were retained as instrumental variables. Inverse-variance-weighted (IVW), weighted median, and MR-Egger regression were primarily used to calculate effect size (β) and corresponding standard error (SE). Heterogeneity was estimated by MR-Egger and IVW methods to assess whether a genetic variant's effect on outcome was proportional to its effect on exposure. Directional pleiotropy was estimated via MR-Egger intercept test for the presence of horizontal pleiotropy.

Statistical Analysis

All wet bench data were expressed as mean ± SEM and the statistical analyses were performed with SPSS 16.0. The 2-tailed Student's *t* test was used for parametric data analyses, ANOVA was used to compare the difference between multiple groups. P<0.05 was considered to be statistically significant.

Results

Single-cell Transcriptomic Analysis Deciphers Differential Cell Types of ApoE$^{-/-}$ and VSMC-iDKO/ApoE$^{-/-}$ Mouse

To understand how epsins in VSMCs might be contributing to lesion development, we initially examined their expressions in lesions with different degrees of atherosclerotic disease burden. In human coronary arteries with

disease classified as normal to mild lesion or in those with large plaques, we observed that epsin1 and epsin2 were highly expressed in VSMCs in the lesion, especially in the severe lesions (Fig. 1A, Extended Data Fig. 1A-B). To further evaluate epsins expression in VSMCs in mouse atherosclerosis, we compared epsins expression in ApoE$^{-/-}$ mice with 16-week normal diet and with 16-week western diet. We found that epsin1 expression was dramatically increased in the plaque of western diet group compared to the normal diet (Extended Data Fig. 1C-D). Besides, we assessed epsins expressions in primary VSMCs isolated from ApoE$^{-/-}$ mice in vitro and found that oxLDL treatment of VSMCs resulted in a 1.9- and 1.7-fold increase in *epsin1* and *epsin2* gene expression, respectively (Extended Data Fig. 1E-F). Together, these observations indicated the potential role of epsins, especially epsin1, involved in atherosclerotic plaques formation.

To determine the biological mechanism of epsins in atherosclerosis, we performed scRNA-seq analysis of atherosclerotic aortas derived from ApoE$^{-/-}$ and tamoxifen injected VSMC-iDKO/ApoE$^{-/-}$ (ApoE$^{-/-}$; Epn1$^{fl/fl}$; Epn2$^{-/-}$; Myh11^{Cre+}) mice fed a western diet for different periods (0, 6,12 and 16 weeks, respectively; Extended Data Fig. 1G-H). Using epsin1 and epsin2 antibodies, we demonstrated epsin1 and epsin2 knockdown in both the lesion and VSMC layer (Extended Data Fig. 3E). After stringent quality control of scRNA-seq data processing, a total of 156,523 cells across week feeding groups (Extended Data Fig. 1I-J), i.e., ApoE$^{-/-}$: ND (n = 23,740), 6-week WD (n = 6,342), 12-week WD (n = 28,345), and 16-week WD (n = 24,061); VSMC-iDKO/ApoE$^{-/-}$: ND (n = 16,073), 6-week WD (n = 21,119), 12-week WD (n = 16,045), and 16-week WD (n = 20,898), were retained for downstream analysis. Graph-based clustering and canonical cell marker annotation revealed eight major cell types with a total of 10 subtypes, i.e., SMC, modSMC (including modSMC-EC, modSMC-myofibroblast), fibroblast, EC, macrophage, immune cell, erythrocyte, and proliferation cell (Fig. 1B, Extended Data Fig. 2A-B). Notably, the compositions of these cell types differed between ApoE$^{-/-}$ and VSMC-iDKO/ApoE$^{-/-}$ mouse across different feeding-week, for which main cell proportions of macrophage were increased along with long-term WD feeding while SMC decreased; the proportion of modSMC-myofibroblast and modSMC-EC were dramatically higher in VSMC-iDKO/ApoE$^{-/-}$ mouse compared with that in ApoE$^{-/-}$ mouse along with long-term WD feeding while macrophage reversed (Fig. 1C, Extended Data Fig. 2C).

In addition, we retrieved coronary artery disease (CAD) GWAS summary statistics in European populations and calculated GWAS signature score of 68 CAD susceptibility genes to map scRNA (Extended Data Fig. 2D), which was significantly lower in VSMC-iDKO/*ApoE*$^{-/-}$ mouse (Fig. 1D, Extended Data Fig. 2E). Further, we observed dramatically differential biological pathways between ApoE$^{-/-}$ and VSMC-iDKO/ApoE$^{-/-}$ mouses across feeding-week (**SupplTable 1**), particularly in 16-week WD feeding that MARK signaling and PDGF-BB signaling involved in SMC transmission were dysregulated against iDKO

treatment (Fig. 1E).

To understand the potential convergent transitions of VSMC to other cells, we performed unsupervised trajectory analysis using RNA velocity algorithms. In ApoE$^{-/-}$ mouse model, we found that VSMC could be transitioned to cell types of modSMC (including modSMC-myofibroblast, modSMC-fibroblast and modSMC-EC) (Fig. 2A, Extended Data Fig. 3A); however, by comparison, the transition of VSMC to macrophage seems to be dampened in VSMC-iDKO/ApoE$^{-/-}$ mouse, thus accelerating the transition to modSMC relevant cell types. As the transition was much more notable in the long-term WD feeding (Fig. 2A), along with the biological alteration (Fig. 1A), we further focused on the 16-week WD feeding models to decipher the SMC transition. The cytoTRACE provided a similar dynamic transcriptional reprogramming starting from VSMC underlying a long-term WD feeding, especially that the predicted cytoTRACE score of modSMC relevant cells were significantly lower in VSMC-iDKO/ApoE$^{-/-}$ mouse compared with that in ApoE$^{-/-}$ mouse, indicating the higher differentiation and more stabilization of these cells induced by DKO treatment (Fig. 2B, Extended Data Fig. 3B). In addition, we performed an unsupervised pseudotime analysis with the above findings for the transitions from SMC to modSMC-myofibroblast and modSMC-EC, respectively (Extended Data Fig. 3C), and notably identified an inverse transition between VSMC and modSMC-EC across ApoE$^{-/-}$ and iDKO/ApoE$^{-/-}$ mouse models (Fig. 2C). Besides, we observed the differential expression pattern of canonical markers (i.e., *Acta2*, and *Pecam1*) across the transitioned cell types between mouse models in the long-term WD feeding (Fig. 2D). Further, cellular interaction analysis indicated that iDKO treatment altered the globally predicted interactions by suppressing number but promoting strength of intercellular interactions (Extended Data Fig. 3D). Also, iDKO treatment differentiated several SMC transition relevant signaling networks (Extended Data Fig. 3E). For example, PECAM1 signaling was dramatically augmented during SMC transition when ApoE$^{-/-}$ mouse received iDKO treatment (Fig. 2E). These findings suggest that the SMC transition during the plaque formation caused by WD feeding might be affected via the knockout of epsins.

Epsins Absent in VSMCs Maintained the Contractile Phenotype and Selectively Increased VSMC Transition to Endothelial-Like Cells

VSMCs were distinguished from other cell types by expression of a unique repertoire of genes including *Acta2*, *Calponin* (*Cnn1*), *Tagln*, and *Myh11* (Extended Data Fig. 2A), which are coordinately down-regulated during phenotypic switching[4].). To verify the scRNAseq results that the proportion of contractile SMCs were dramatically higher in VSMC-iDKO/ApoE$^{-/-}$ mice than that in ApoE$^{-/-}$ mice, we harvested aorta from ApoE$^{-/-}$ mice and tamoxifen injected VSMC-iDKO/ApoE$^{-/-}$ mice with 16 weeks of western diet, and observed that VSMC markers related to VSMC contraction and phenotype (i.e., *Acta2*, *Cnn1*, *Tagln*, and *Myh11*) were significantly enriched in the aorta of tamoxifen

injected VSMC-iDKO/ApoE$^{-/-}$ mice (Extended Data Fig. 4A). Notably, epsin1/2 were associated with the suppression in VSMC marker genes as determined by both immnuo-blotting and immuno-staining (Fig. 3A-B, Extended Data Fig. 4A). To extend our studies showing epsins associated suppression of VSMC differentiation marker genes in vivo, aortic VSMCs isolated from ApoE$^{-/-}$ mice and tamoxifen injected VSMC-iDKO/ApoE$^{-/-}$ mice were treated with 100 μg/mL oxLDL for 72 h, followed by western blot. The upstream VSMC markers expression, including α-SMactin, Calponin1, SM22 and MyH11, were already suppressed maximally with 72 h oxLDL treatment, and no suppression could be achieved in epsins specific knockout in VSMCs (Extended Data Fig. 5C). Taken together, our study uncovered a novel and critical role for Epsin in regulating VSMC phenotype switching by atherogenic stimuli.

scRNA seq results showed that in atherosclerotic plaques, VSMC-markers positive cells were observed to comprise significant proportions of contractile VSMCs, modSMC-EC, modSMC-monocytes/macrophage, modSMC-myofibroblast, fibroblasts, macrophages, and smaller proportions of endothelial and other cell types (Extended Data Fig. 3A-C), which is supported by Pan et al[14]. And VSMCs may take on each of these phenotypic states[36]. To determine the role of epsin1/2 in regulating the VSMC phenotype transition to endothelial-like cells (i.e., modSMC-EC cell type in scRNA), we detected the endothelial-related marker CD31 in aorta and VSMCs isolated from ApoE$^{-/-}$ mice and tamoxifen injected VSMC-iDKO/ApoE$^{-/-}$ mice. Endothelial-related marker CD31 was found to be overrepresented in tamoxifen injected VSMC-iDKO/ApoE$^{-/-}$ mice (Fig. 3A, Extended Data Fig. 4B). To track VSMC-transdifferentiated endothelial-like cells in atherogenesis, we generated epsin1/2 specific knockout VSMC-lineage tracing murine model (Extended Data Fig. 1G). Immune-staining with both CD31 and VE-Cadherin in atherosclerotic brachiocephalic arteries (BCA) \sections from VSMC lineage tracing mice showed a marked increase of CD31 and VE-Cadherin-stained VSMC cells in VSMC-iDKO/YFP$^{+/-}$/ApoE$^{-/-}$ mice (Fig. 3D, Extended Data Fig. 4C-D). Fibroblast cells and macrophages were also localized using immune-staining with fibroblast marker Ecrg4 and macrophage marker Lgals3 within atherosclerotic lesions in VSMC-YFP-tagged mice. In BCA sections of 16-week WD fed VSMC-iDKO/YFP$^{+/-}$/ApoE$^{-/-}$ mice, there were less YFP^{+} Ecrg4^{+} and YFP^{+} Lgals3^{+} cells localized in media of the lesion, with some cells localized in intima overlying the media (Extended Data Fig. 4E-F). Similar results were obtained from the sorted VSMCs with YFP-tag by flow cytometric evaluations. The proportion of YFP^{+} cells in intima, containing scattered modSMC cells, was 0.98% in YFP$^{+/-}$/ApoE$^{-/-}$ mice and 3.03% in VSMC-iDKO/YFP$^{+/-}$/ApoE$^{-/-}$ mice for CD31 (Fig. 3E), and 2.18% in YFP$^{+/-}$/ApoE$^{-/-}$ mice and 3.89% in VSMC-iDKO/YFP$^{+/-}$/ApoE$^{-/-}$ mice for VE-Cadherin (Fig. 4G). Together, these findings indicated that epsins played opposing roles in regulating VSMC contractile phenotype, VSMC-derived endothelial-like cells and VSMC de-differentiation to fibroblast- and macrophages-like cells.

To further understand the impact of epsins on endothelial-like cells differentiated from VSMCs, we further co-stained primary aortic VSMCs with αSMA and multiple endothelial-related markers. Under the confocal, EC-markers positive cells (CD31 and NRP1) can be observed in epsins specific knockout VSMCs, and the cell morphology were changed toward to EC (Extended Data Fig. 5D).

Utilizing single-cell genomics to interrogate VSMC de-differentiation during atherosclerosis, Pan et al[14] reported that the cell state marked with EC marker was an intermediate cell state derived from VSMC. Similarly, our scRNAseq results showed that the cell state with EC marker *Pecam1* could not only expressed in ECs, but also in SMCs and SMC-differentiated macrophage-like and myofibroblast-like cells (Fig. 2D, Fig. 3C). One of the classic functions of ECs is to uptake acetylated low-density lipoprotein (ac-LDL) which maintained homeostasis of blood cholesterol concentration[37]. Thus, to evaluate whether ECs differentiated from VSMCs possessed true EC functions, we tested if epsins-specific knockout in VSMCs promoted VSMC-derived endothelial-like cells uptaking ac-LDL. We sorted VSMCs with YFP-tagged from the aortic root through the iliac bifurcation of YFP-VSMC/ApoE$^{-/-}$ and YFP-VSMC-iDKO/ApoE$^{-/-}$ mice. The sorted freshly dissociated cells were treated with Dil-ac-LDL for 5 h following by immune-staining with endothelial markers CD31 or VE-Cadherin. We observed increased YFP-tagged VSMCs with Dil-ac-LDL and CD31/VE-Cadherin coming from YFP-VSMC-iDKO/ApoE$^{-/-}$ mice, indicating that epsins deficiency in VSMCs inducing VSMC phenotype transition to endothelial-like cells with EC function (Fig. 3F, Extended Data Fig. 5A-B). In line with these observations, the application of Dil-ac-LDL to cultured primary VSMCs resulted in an increase in VSMC-iDKO/ApoE$^{-/-}$ group ($P<0.0001$ vs ApoE$^{-/-}$ group) (Extended Data Fig. 5E). Taken together, these data suggested that epsins-specific knockout in VSMCs induced VSMC transdifferentiating to endothelial-like cells and these endothelial-like cells were functional because the cells were localized in intima overlying the media and correlated with an increase of ac-LDL ingestion.

Epsins Suppress the Expression of VSMC markers by Decreasing KLF4 Expression

It was shown that KLF4 is required for both VSMCs phenotypic transitions within atherosclerotic lesions[5], and participated in the VE-cadherin promoter activity in ECs[38]. In this study, we postulated that KLF4 would play a key role in VSMC conditional knockout of *epsins* induced marked increase in VSMC-transdifferentiated endothelial-like cells. Initially, considering the enrichment of KLF4 in extracellular space, we performed a Mendelian Randomization analysis to evaluate the relationship between KLF4 and CAD risk, and observed that higher level of plasma KLF4 protein was causally associated with increased risk of CAD in the general population (Fig. 4A). As well, KLF4 protein was

increased in severe lesion of human, with the co-localization of VSMCs (Fig. 4B, Extended Data Fig. 6A).

To further explore the role of KLF4 in VSMCs, we next investigated whether atheroprone diet which was known to increase KLF4 expression could induce KLF4 in VSMCs depending on epsins. We observed the dramatically increased KLF4 in ApoE$^{-/-}$ mice with western diet compared with the normal chew diet (Fig. 4C, Extended Data Fig. 6B). Conversely, VSMC-specific epsins knockout decreased western diet induced KLF4 protein abundance (Fig. 4D-E, Extended Data Fig. 6C-D), but not affect the KLF4 mRNA expression (Extended Data Fig. 6E) between ApoE-/- and VSMC-iDKO/ApoE-/- groups, indicating that KLF4 is post-transcriptional regulated by epsins. In addition, we sorted VSMCs from 16-week western diet fed lineage tracing mice to the expression of KLF4. Both flow cytometric analyses and confocal microscope showed that about 90.1% of VSMCs were KLF4 positive in YFP-VSMC/ApoE$^{-/-}$ mice, but only 66.5% in YFP-VSMC-iDKO/ApoE$^{-/-}$ mice (Fig. 4F-G, Extended Data Fig. 6F). By using primary VSMCs isolated from mice with VSMC-specific epsins knockout, we observed significantly lower KLF4 expression in VSMCs from VSMC-iDKO/ApoE$^{-/-}$ mice than that from ApoE$^{-/-}$ controls (Fig. 4J, Extended Data Fig. 6G). Similarly, immunofluorescence staining showed that KLF4 expression in primary VSMCs was induced and abundant KLF4 transferred into nucleus in VSMC with epsins existing after oxLDL treatment (Extended Data Fig. 6H). These data indicated that epsins were crucial for the protein level of KLF4 in VSMCs.

To further explore whether KLF4 could modulate the suppress function of epsins on the expression of VSMC differentiation markers as well as VSMC-to-endothelial transition (MEndoT), we performed CUT&Tag profiling against KLF4 in ApoE$^{-/-}$ and VSMC-iDKO/ApoE$^{-/-}$ mice models. After comparing differential binding peaks between two types mice, we retrieved 1113 target genes from KLF4 array and mapped them to scRNA as KLF4 binding gene signature (**SupplTable 2**). Intriguingly, we observed that the KLF4 binding gene signature score was lower in VSMC-iDKO/ApoE$^{-/-}$ mice than that in ApoE$^{-/-}$ mice underlying a long-term WD feeding (Fig. 4I), especially in cell types of SMC, modSMC-EC, modSMC-myofibroblast, and macrophage cells (Extended Data Fig. 6I). In parallel, we detected the expression pattern of VSMC markers from VSMC-iDKO/ApoE$^{-/-}$ mice with adenovirus-mediated overexpression of KLF4 (Ad-KLF4) in comparison with empty vector (Ad-null) and observed that all VSMC markers (i.e., *Tagln*, *Acta2*, *Cnn1*, and *MyH11*) were dramatically suppressed by Ad-KLF4 against KLF4 over-expression (Extended Data Fig. 6J). Together, these findings suggest that loss of epsins in VSMCs attributed to the inhibition of VSMC contractile phenotype switching in atherosclerosis through both promoting KLF4 translocation into nuclei and downregulating KLF4 expression.

Epsins promote the stability of KLF4 and hinders KLF4 ubiquitination via

preventing VHL binding to KLF4

To explore the mechanism how epsins upregulated KLF4 expression by atherogenic stimuli, we performed coimmunoprecipitations from lysates of primary VSMCs from ApoE$^{-/-}$and VSMC-iDKO/ApoE$^{-/-}$ mice treated with oxLDL. As shown in Fig. 4J, KLF4 expression was repressed in VSMCs from VSMC-iDKO/ApoE$^{-/-}$ mice, and there was an interaction between epsin1 and KLF4 which could be enhanced by oxLDL treatment (Extended Data Fig. 6K). Emerging evidence revealed that KLF4 was unstable and regulated by ubiquitination[39]. To determine whether epsin could govern KLF4 stability in VSMCs in atherosclerosis, we treated VSMCs with the proteasomal inhibitor, MG132, to impair KLF4 degradation, following with oxLDL for 24 h, then lysed the cells, immunoprecipitated KLF4 and analysed KLF4 ubiquitination by western blot. Notably, epsins depletion decreased KLF4 expression, while KLF4 polyubiquitination was induced after MG132 + oxLDL treatment (Fig. 4K, Extended Data Fig. 7A-B), suggesting that epsins improved the stability of KLF4 via repressing KLF4 degradation through downregulating the polyubiquitination of KLF4 to increase KLF4 expression (Fig. 4H).

Our previous studies reported epsins could recognize ubiquitinated cell via its ubiquitin-interacting motif (UIM) domain[16,17]. To determine that epsin domains were responsible for the interaction which contributed to improve the stability of KLF4, we created HA-tagged mammalian epsin1 wild-type full length and ENTH, UIM or ENTH+UIM deletion constructs (HA-Epsin1^{WT}, HA-Epsin1$^{\triangle ENTH}$, HA-Epsin1$^{\triangle UIM}$ or HA-Epsin1$^{DPW/NPF}$). We transfected these constructs to HEK 293T cells and performed coimmunoprecipitation with KLF4. UIM domain of Epsin1 played a leading role in the interaction between Epsin1 and KLF4 as the binding between Epsin1$^{\triangle UIM}$ and KLF4 was dramatically reduced in HA-Epsin1$^{\triangle UIM}$-expressing cells, but there was nearly no interaction in HA-Epsin1$^{DPW/NPF}$-expressing cells, suggesting the interaction was partly through ENTH domain (Fig. 4L, Extended Data Fig. 7C). Taken together, epsins preserved the stability of KLF4 through inhibiting KLF4 degradation mediated by ubiquitination via binding between Epsin1 ENTH+UIM domain and KLF4.

It is reported that KLF4 ubiquitination is catalyzed by VHL, an E3 ubiquitin ligase for proteasomal degradation, in breast cancer[40]. We hypothesized that epsins reduced KLF4 ubiquitination by interfering with the interaction between VHL and KLF4. Firstly, we observed that both *Vhl* and *Klf4* expressions in VSMC of scRNA data were significantly correlated and increased in long-term WD feeding (Extended Data Fig. 7D), which indicated the interaction of VHL and KLF4 proteins beyond the RNA level. We further used immunofluorescence to analyze VHL protein in human tissue sections containing atherosclerotic lesions and observed that VHL upregulation correlated strongly with increased atherosclerosis severity (Extended Data Fig. 7E). In addition, we found that VHL protein was upregulated by oxLDL, and epsin deficiency significantly increased VHL protein in VSMCs (Extended Data Fig. 7F,G). To determine whether epsins impacted the interaction between VHL and KLF4, we performed co-

immunoprecipitation assays in epsins specific knockout in VSMCs using VHL-specific antibody and found that more VHL bound KLF4 after oxLDL treatment, epsin loss also significantly enhanced the interaction between VHL and KLF4 (Extended Data Fig. 7F,H), further suggesting loss of epsins reduced KLF4 expression by interfering with the interaction between VHL and KLF4.

Epsins inhibit the expression of EC markers in VSMCs by decreasing the Oct4 expression

Our study provided evidence that epsins loss in VSMCs played an atheroprotective role by decreasing inflammation via augmenting KLF4 degradation, however, KLF4 did not affect VSMC-specific epsins deficiency induced VSMC-transdifferentiated endothelial-like cells in atherogenesis (Fig. 6, Extended Data Fig. 6K). Owens GK et al. have identified that Klf4 and Oct4 control nearly opposite patterns of gene expression in VSMC and KLF4 or Oct4 target genes that may impact VSMC phenotypic transitions[41]. To address the role of Oct4 in VSMC transition into endothelial-like cells, we firstly enriched OCT4 binding gene signature that was calculated by 898 genes derived from CUT&Tag array (**SupplTable 2**) and found that OCT4 binding gene signature score in both SMC and modSMC-EC was significantly higher in VSMC-iDKO/ApoE$^{-/-}$ mice than that in ApoE$^{-/-}$ mice (**Fig. 5A**). Subsequently, we detected Oct4 expression in ApoE$^{-/-}$ and VSMC-iDKO/ApoE$^{-/-}$ mouse models and found no difference of *Oct4* expression in SMC cell clusters between ApoE$^{-/-}$ and VSMC-iDKO/ApoE$^{-/-}$ mouse models (Extended Data Fig. 8A), while *Oct4* expression was higher in the aorta from VSMC-iDKO/ApoE$^{-/-}$ mouse models (Extended Data Fig. 8B), as well as at the protein level (Fig. 5B, Extended Data Fig. 8C). Furthermore, we saw increased protein levels of Oct4 in aortic arch, thoracic aorta and abdominal aorta from VSMC-iDKO/ApoE$^{-/-}$ mice compared with ApoE$^{-/-}$ mice, but no change in the different parts of aorta from the same group (Fig. 5C, Extended Data Fig. 8D). By using primary VSMCs with oxLDL treatment, we inferred whether Epsins increased expression of Oct4 in the VSMCs in vitro. As expected, the expression of Oct4 in primary VSMCs was upregulated by epsins knockout (Extended Data Fig. 8E). Then, BCA was collected from VSMC-iDKO/ApoE$^{-/-}$ versus ApoE$^{-/-}$ mice with 16-week western diet to measure Oct4 expression levels in VSMC in the atherosclerotic plaque using immunofluorescent staining with αSMA and Oct4 antibodies. We observed the upregulated Oct4 expression which shared the same location with αSMA antibody marked VSMCs in the lesion of VSMC-iDKO/*ApoE*$^{-/-}$ mice, but little Oct4 expressed in that of ApoE$^{-/-}$ mice (Extended Data Fig. 8F).

Next to assess the possible functional properties of Oct4 in VSMC derived endothelial-like cells, we analyzed BCA lesions from YFP-VSMC-iDKO/ApoE$^{-/-}$ and YFP-VSMC/ApoE$^{-/-}$ mice by immuno-staining with antibodies to EC marker CD31 and Oct4. Consistently, there were more cells with Oct4 expression, and Oct4 expressed highly in YFP^{+} CD31^{+} cells localized in the intima of plaque (Fig. 5D, Extended Data Fig. 8G). Furthermore, we performed flow cytometry

analysis on VSMC with YFP tag from YFP-VSMC-iDKO/ApoE$^{-/-}$ and YFP-VSMC/ApoE$^{-/-}$ mice, observed that about 2.71% of VSMCs were Oct4 positive in YFP-VSMC-iDKO/ApoE$^{-/-}$ mice, proportion is only 0.63% in YFP-VSMC/ApoE$^{-/-}$ mice (Fig. 5E). In addition, we sorted YFP-tagged VSMCs from lineage tracing mice with 16-week western diet to test the Oct4 expression in VSMCs and the relationship between Oct4 and VSMC-derived endothelial-like cells. The results showed that there were more Oct4+ and CD31+ or VE-Cadherin+ cells in YFP-tagged VSMCs sorted from YFP-VSMC-iDKO/ApoE$^{-/-}$ than that from YFP-VSMC/ApoE$^{-/-}$ mice, and most of the Oct4+ and CD31+ or VE-Cadherin+ cells shared the same location (Fig. 5F), suggesting that Oct4 might play a role in VSMC-derived endothelial-like cells.

To further explore whether Oct4 modulates the suppress function of epsins on the expression of VSMC contractile markers as well as MEndoT, we performed both qRT-PCR and western blot in VSMCs isolated from VSMC-iDKO/ApoE$^{-/-}$ mice with Oct4 siRNA treatment. The results showed that epsins deficiency increased the expression of VSMC contractile and EC markers in VSMCs, which were reversed by Oct4 siRNA induced Oct4 knockout (Fig. 5G-H).

VSMC-Specific Epsins Deficiency Reduces the Size of Atherosclerotic Lesion and Increased the Plaque Stability in Diseased Mice.

Given our observation that epsins expression was upregulated in VSMC in atherosclerotic lesions and VSMC-specific epsins deficiency would selectively increase VSMC transition to endothelial-like cells and decrease the inflammation in response to vascular injury by atherogenic stimuli, we postulated that epsins inhibition in VSMC would reduce atherosclerotic lesion size. To test this, we administered ApoE$^{-/-}$ mice and tamoxifen injected VSMC-iDKO/ApoE$^{-/-}$ mice fed a western diet for 9, 16, 20 weeks. Assessment of the *en face* lesion area in whole aorta revealed that VSMC specific epsin 1 and 2 deficiency significantly reduced lesion development in comparison with ApoE$^{-/-}$ mice (P=0.0012 with 9-week WD, P=0.0247 with 16-week WD, P=0.0003 with 9-week WD, comparison with control ApoE$^{-/-}$ mice; Fig. 6A, Extended Data Fig. 9A). Furthermore, examination of aortic root lesions demonstrated that tamoxifen injected VSMC-iDKO/ApoE$^{-/-}$ mice had a 56.57% reduction in lesion area in comparison with ApoE$^{-/-}$ mice (Fig. 6B, Extended Data Fig. 9B). Using Oil Red O staining, we also observed significant changes in sinus lesion and BCA area (43.16% or 61.14% decrease relative to ApoE$^{-/-}$ mice) (Fig. 6C, Extended Data Fig. 9C-D).

To evaluate the inflammatory profile of the atherosclerotic lesions of these mice, we assessed lesion composition by immunostaining markers of macrophages (CD68) within aortic sinus lesions. Consistent with a reduction in atherosclerotic progression, we detected a reduction in macrophage area by 59.2% in tamoxifen injected VSMC-iDKO/ApoE$^{-/-}$ mice (P<0.0001 vs ApoE$^{-/-}$

mice; Fig. 6D, Extended Data Fig. 9E). Last, we observed a reduction in ICAM-1 and P-selectin staining in the endothelial layer of aortic root lesions of tamoxifen injected VSMC-iDKO/ApoE$^{-/-}$ mice fed with 20-week western diet in comparison with ApoE$^{-/-}$ mice (Extended Data Fig. 9F-G), which was consistent with the decreased inflammation observed in the atherosclerotic plaques of these mice. Together, these data demonstrated that silencing of epsins in VSMC could protect against atherosclerotic progression induced by a western diet.

In addition to reduction of lesion size, the constitution of a thick fibrous cap is an important feature of plaque stabilization that can prevent physical plaque disruption and subsequent thrombus formation. Indeed, in fatal myocardial infarction, the plaque has a large necrotic core, a relative paucity of VSMCs, a thin collagen fibrous cap and more dead cells[42]. Our scRNAseq results showed that loss of epsins in VSMCs increased the SMC-derived myofibroblast which is benefit to the protective fibrous cap formation[10](Fig. 1D, Extended Data Fig. 2D). To ascertain plaque stability, we analyzed the size of necrotic core, plaque collagen content, accumulation of contractile VSMC content and dead cell content in tamoxifen injected VSMC-iDKO/ApoE$^{-/-}$ mice. Epsins specific knockout in VSMCs significantly reduced the necrotic core area/total plaque area ratio as determined by staining for hematoxylin and eosin staining (Fig. 6E), and elevated plaque collagen content as determined by staining for Van Gieson's staining, and Van Gieson's Red dramatic increase in collagen content (Fig. 6F), and accompanied by an decrease in dead cell content which is marked by cleaved-Caspase3 (Fig. 6G, Extended Data Fig. 9H) in atherosclerotic lesions.

To determine whether specific loss of epsins in VSMCs would alter the accumulation of contractile VSMCs in atherosclerotic plaques, we stained cross-sections of aortic root with the VSMC marker αSMA, and stained cross-sections of BCA with VSMC markers, αSMA, SM22, Calponin1 and Myh11. The tamoxifen injected VSMC-iDKO/*ApoE*$^{-/-}$ mice showed a marked increase in the αSMA-positive VSMC area in the atherosclerotic lesions of aortic root and BCA, especially on the top of the lesion area (Fig. 6H, 3B). Areas of plaques that stained positive for αSMA were also positive for SM22, Calponin1 and Myh11 (Fig. 3B). Concordant with these in vivo observations, epsins-knockout enhanced α-SMA expression in cultured VSMCs (Extended Data Fig. 5D). Together, Epsins specific deletion in VSMCs could have an additional beneficial effect on the stability of atherosclerotic plaque.

Discussion

Several studies have demonstrated endothelial epsins could exacerbate endothelial dysfunction associated with atherosclerosis[15,16], and epsins in macrophages contributed to the progression of atherosclerosis as well [17,43]. However, the role of epsins in VSMCs involving atherosclerosis throughout all

stages remain unknown. In this study, we discovered that epsin expression levels in VSMCs tightly correlated with the severity of atherosclerosis in both human and mouse atherosclerotic tissues. Notably, selective loss of *epsin1 and 2* within VSMCs could reduce lesion size and lipid loading, increase fibrous cap thickness, and decline in the proportion of VSMC-derived macrophage- and fibroblast-like cells but increase in *Myh11+* and *Acta2+* cells within the fibrous cap. By integrating scRNAseq data with GWAS, we discovered that epsin knockout in VSMCs suppressed the expression of CAD susceptibility genes, highlighting the pivotal of VSMC-epsins in the development of CAD. Using single-cell genomics, VSMC-specific epsins mutant mice and lineage tracing mice to interrogate the role of epsins in the dynamics of SMC phenotypic modulation during atherosclerosis, we revealed VSMCs can transdifferentiate into endothelial-like cell state, with the loss of epsins resulting in a higher proportion of SMC-derived endothelial-like cells and myofibroblast, particularly in advanced atherosclerotic lesions. We confirmed these findings utilizing multiple methods at both mRNA and protein levels.

Previous studies reported SMC-derived *Vcam+* cells, which were assumed to be SEMs (stem cell, endothelial cell and monocytes/macrophage differentiation, termed de-differentiated VSMCs) defined as an intermediate cell state, in human atherosclerotic plaques and mouse atherosclerotic models[14]. Of greatest significance, through series trajectory analyses, we show that the absence of epsins not only increased an inverse transition between SMC and modSMC-EC, but also resulted in a higher differentiation and more stabilization of SMC-derived endothelial-like cells. By harnessing lineage tracing mice, cell sorting and endothelial functional assessment, we revealed that SMC-derived endothelial-like cells can perform the functions of endothelial cells. Taken together, our studies point toward that the molecular features of SMC-derived endothelial-like cells are not simply intermediate cell state, but a unique transition state from VSMCs found in the milieu of atherosclerosis, which has the potential to restore the dysfunctional endothelium, suggesting clinical relevance of this cell state.

In this study, Mendelian Randomization analysis showed that the elevated plasma KLF4 protein can act as a risk factor of CAD in the general population. Consistently, KLF4 in VSMCs was abundant in both human and mouse atherosclerotic lesions, exhibiting parallel upregulation with epsins. The highly expressed KLF4 in response to atherogenic stimuli was attenuated in the absence of epsins. Given epsins' classical role as a membrane-associated endocytic adaptor, they were dispensable for *KLF4* transcription. The protein expression of KLF4 is downregulated after KLF4 exporting from nuclear localization to a cytoplasmic localization in mouse blastocysts[44]. In an epsins deletion-specific context, KLF4 nuclei expression were reduced in oxLDL treated VSMCs, suggesting that epsins is critical for maintaining KLF4 in the nuclei. In contractile VSMCs, KLF4 expression is balanced by protein ubiquitination governed by VHL ubiquitin-protein ligase and subsequent

degradation[45]. In light of our extensive mechanistic binding analyses, we propose a model in which epsin interacts constitutively with KLF4 via its UIM and ENTH domains, presumably maintaining KLF4 in nuclei to escape from VHL E3 ligase binding, and thus reducing KLF4 ubiquitination and degradation. Our results provide a potential explanation for why epsins and KLF4 are correspondingly upregulated in both human and mouse atherosclerotic tissues.

Klf4 as a transcription factor has been implicated to be involved in VSMC phenotype modulation[5,46]. However, in each VSMC phenotype, the role of KLF4 respect to gene regulation and transcription factor cooperation is distinct and context-dependent[47-49]. In our study, we show that phenotypically modulated SMCs differentiate to multiple phenotypes including cells that express markers of fibroblast, macrophage, and endothelial cell in mouse atherosclerotic model. KLF4 overexpression regressed the marked reductions in contractile VSMCs phenotype, which were resulted by loss of epsins within VSMCs, while endothelial-like VSMC phenotype showed no response to the upregulated KLF4 expression.

Additionally, KLF4 functions as a scaffolding protein platform to recruit other transcriptional regulators to SMC gene promoters, responding to different environmental cues[50]. KLF4/Oct4 complex is sufficient but necessary to generate induced pluripotent stem cells from several cell types, such as dermal papilla cells and adult neural stem cells[51, 52,53]. However, It is reported that loss of Oct4 within VSMC had virtually completely opposite overall effects on lesion pathogenesis in the present studies as compared to SMC specific loss of Klf4[41]. KLF4 and Oct4 are functional in controlling opposite aspects of SMC phenotypic transitions in the atherosclerotic context[5,54]. In our final observations, we found that VSMC epsins deficiency suppress the KLF4 expression while abundant Oct4 in VSMC-drived endothelial-like cells. Loss of Oct4 in VSMCs resulted in more VSMC markers and EC marker expression. These findings need to be confirmed in further comprehensive mechanism studies. In addition, a future study will be conducted to comprehensively evaluate the predictive value of the therapeutic effects of epsins siRNAs containing nanoparticles to precisely target lesional VSMCs on atherosclerosis progression.

In summary, our study reveals a novel cell state during VSMC phenotypic switching and identifies potential therapeutic targets to repair the dysfunctional endothelium for atherosclerosis. Epsins are critical for VSMC dedifferentiation and atherosclerosis progression by protecting KLF4 from ubiquitination and proteasomal degradation. The absence of epsins in VSMCs resulted in the loss of KLF4 and decreased the progression of atherosclerosis in VSMC-iDKO/*ApoE*$^{-/-}$ mice. These insights may pave the way for targeted VSMC-epsin inhibition as a novel therapeutic treatment of CAD.

References

1 Kong, P. *et al.* Inflammation and atherosclerosis: signaling pathways and therapeutic intervention. *Signal Transduct Target Ther* **7**, 131, doi:10.1038/s41392-022-00955-7 (2022).

2 Frak, W. *et al.* Pathophysiology of Cardiovascular Diseases: New Insights into Molecular Mechanisms of Atherosclerosis, Arterial Hypertension, and Coronary Artery Disease. *Biomedicines* **10**, doi:10.3390/biomedicines10081938 (2022).

3 Bennett, M. R., Sinha, S. & Owens, G. K. Vascular Smooth Muscle Cells in Atherosclerosis. *Circ Res* **118**, 692-702, doi:10.1161/CIRCRESAHA.115.306361 (2016).

4 Gomez, D. & Owens, G. K. Smooth muscle cell phenotypic switching in atherosclerosis. *Cardiovasc Res* **95**, 156-164, doi:10.1093/cvr/cvs115 (2012).

5 Shankman, L. S. *et al.* KLF4-dependent phenotypic modulation of smooth muscle cells has a key role in atherosclerotic plaque pathogenesis. *Nat Med* **21**, 628-637, doi:10.1038/nm.3866 (2015).

6 Chappell, J. *et al.* Extensive Proliferation of a Subset of Differentiated, yet Plastic, Medial Vascular Smooth Muscle Cells Contributes to Neointimal Formation in Mouse Injury and Atherosclerosis Models. *Circ Res* **119**, 1313-1323, doi:10.1161/CIRCRESAHA.116.309799 (2016).

7 Wong, D., Turner, A. W. & Miller, C. L. Genetic Insights Into Smooth Muscle Cell Contributions to Coronary Artery Disease. *Arterioscler Thromb Vasc Biol* **39**, 1006-1017, doi:10.1161/ATVBAHA.119.312141 (2019).

8 Sabatine, M. S. *et al.* Evolocumab and Clinical Outcomes in Patients with Cardiovascular Disease. *N Engl J Med* **376**, 1713-1722, doi:10.1056/NEJMoa1615664 (2017).

9 Basatemur, G. L., Jorgensen, H. F., Clarke, M. C. H., Bennett, M. R. & Mallat, Z. Vascular smooth muscle cells in atherosclerosis. *Nat Rev Cardiol* **16**, 727-744, doi:10.1038/s41569-019-0227-9 (2019).

10 Wirka, R. C. *et al.* Atheroprotective roles of smooth muscle cell phenotypic modulation and the TCF21 disease gene as revealed by single-cell analysis. *Nat Med* **25**, 1280-1289, doi:10.1038/s41591-019-0512-5 (2019).

11 Dobnikar, L. *et al.* Disease-relevant transcriptional signatures identified in individual smooth muscle cells from healthy mouse vessels. *Nat Commun* **9**, 4567, doi:10.1038/s41467-018-06891-x (2018).

12 Feil, S. *et al.* Transdifferentiation of vascular smooth muscle cells to macrophage-like cells during atherogenesis. *Circ Res* **115**, 662-667, doi:10.1161/CIRCRESAHA.115.304634 (2014).

13 Jovic, D. *et al.* Single-cell RNA sequencing technologies and applications: A brief overview. *Clin Transl Med* **12**, e694, doi:10.1002/ctm2.694 (2022).

14 Pan, H. *et al.* Single-Cell Genomics Reveals a Novel Cell State During Smooth Muscle Cell Phenotypic Switching and Potential Therapeutic Targets for Atherosclerosis in Mouse and Human. *Circulation* **142**, 2060-2075, doi:10.1161/CIRCULATIONAHA.120.048378 (2020).

15 Dong, Y. *et al.* Targeting Epsins to Inhibit Fibroblast Growth Factor Signaling While Potentiating Transforming Growth Factor-beta Signaling Constrains Endothelial-to-Mesenchymal Transition in Atherosclerosis. *Circulation* **147**, 669-685, doi:10.1161/CIRCULATIONAHA.122.063075 (2023).

16 Dong, Y. *et al.* Epsin-mediated degradation of IP3R1 fuels atherosclerosis. *Nat Commun* **11**, 3984, doi:10.1038/s41467-020-17848-4 (2020).

17 Cui, K. *et al.* Epsin Nanotherapy Regulates Cholesterol Transport to Fortify Atheroma Regression. *Circ Res* **132**, e22-e42, doi:10.1161/CIRCRESAHA.122.321723 (2023).

18 Salmon, M., Gomez, D., Greene, E., Shankman, L. & Owens, G. K. Cooperative binding of KLF4, pELK-1, and HDAC2 to a G/C repressor element in the SM22alpha promoter mediates transcriptional silencing during SMC phenotypic switching in vivo. *Circ Res* **111**, 685-696, doi:10.1161/CIRCRESAHA.112.269811 (2012).

19 Hu, D. *et al.* Interplay between arginine methylation and ubiquitylation regulates KLF4-mediated genome stability and carcinogenesis. *Nat Commun* **6**, 8419, doi:10.1038/ncomms9419 (2015).

20 Kawai-Kowase, K. *et al.* PIAS1 mediates TGFbeta-induced SM alpha-actin gene expression through inhibition of KLF4 function-expression by protein sumoylation. *Arterioscler Thromb Vasc Biol* **29**, 99-106, doi:10.1161/ATVBAHA.108.172700 (2009).

21 Adam, P. J., Regan, C. P., Hautmann, M. B. & Owens, G. K. Positive- and negative-acting Kruppel-like transcription factors bind a transforming growth factor beta control element required for expression of the smooth muscle cell differentiation marker SM22alpha in vivo. *J Biol Chem* **275**, 37798-37806, doi:10.1074/jbc.M006323200 (2000).

22 Stuart, T. *et al.* Comprehensive Integration of Single-Cell Data. *Cell* **177**, 1888-1902 e1821, doi:10.1016/j.cell.2019.05.031 (2019).

23 Korsunsky, I. *et al.* Fast, sensitive and accurate integration of single-cell data with Harmony. *Nat Methods* **16**, 1289-1296, doi:10.1038/s41592-019-0619-0 (2019).

24 La Manno, G. *et al.* RNA velocity of single cells. *Nature* **560**, 494-498, doi:10.1038/s41586-018-0414-6 (2018).

25 Bergen, V., Lange, M., Peidli, S., Wolf, F. A. & Theis, F. J. Generalizing RNA velocity to transient cell states through dynamical modeling. *Nat Biotechnol* **38**, 1408-1414, doi:10.1038/s41587-020-0591-3 (2020).

26 Gulati, G. S. *et al.* Single-cell transcriptional diversity is a hallmark of developmental potential. *Science* **367**, 405-411, doi:10.1126/science.aax0249 (2020).

27 Qiu, X. *et al.* Reversed graph embedding resolves complex single-cell trajectories. *Nat Methods* **14**, 979-982, doi:10.1038/nmeth.4402 (2017).

28 Jin, S. *et al.* Inference and analysis of cell-cell communication using CellChat. *Nat Commun* **12**, 1088, doi:10.1038/s41467-021-21246-9 (2021).

29 Nelson, C. P. *et al.* Association analyses based on false discovery rate implicate new loci for coronary artery disease. *Nat Genet* **49**, 1385-1391, doi:10.1038/ng.3913 (2017).

30 Nikpay, M. *et al.* A comprehensive 1,000 Genomes-based genome-wide association meta-analysis of coronary artery disease. *Nat Genet* **47**, 1121-1130, doi:10.1038/ng.3396 (2015).

31 Myocardial Infarction, G. *et al.* Coding Variation in ANGPTL4, LPL, and SVEP1 and the Risk of Coronary Disease. *N Engl J Med* **374**, 1134-1144, doi:10.1056/NEJMoa1507652 (2016).

32 de Leeuw, C. A., Mooij, J. M., Heskes, T. & Posthuma, D. MAGMA: generalized gene-set analysis of GWAS data. *PLoS Comput Biol* **11**, e1004219, doi:10.1371/journal.pcbi.1004219 (2015).

33 Ferkingstad, E. *et al.* Large-scale integration of the plasma proteome with genetics and disease. *Nat Genet* **53**, 1712-1721, doi:10.1038/s41588-021-00978-w (2021).

34 Burgess, S. *et al.* Guidelines for performing Mendelian randomization investigations: update for summer 2023. *Wellcome Open Res* **4**, 186, doi:10.12688/wellcomeopenres.15555.3 (2019).

35 Hemani, G. *et al.* The MR-Base platform supports systematic causal inference across the human

phenome. *Elife* **7**, doi:10.7554/eLife.34408 (2018).

36 Conklin, A. C. *et al.* Meta-Analysis of Smooth Muscle Lineage Transcriptomes in Atherosclerosis and Their Relationships to In Vitro Models. *Immunometabolism* **3**, doi:10.20900/immunometab20210022 (2021).

37 Hassan, H. H., Denis, M., Krimbou, L., Marcil, M. & Genest, J. Cellular cholesterol homeostasis in vascular endothelial cells. *Can J Cardiol* **22 Suppl B**, 35B-40B, doi:10.1016/s0828-282x(06)70985-0 (2006).

38 Cowan, C. E. *et al.* Kruppel-like factor-4 transcriptionally regulates VE-cadherin expression and endothelial barrier function. *Circ Res* **107**, 959-966, doi:10.1161/CIRCRESAHA.110.219592 (2010).

39 Chen, Z. Y., Wang, X., Zhou, Y., Offner, G. & Tseng, C. C. Destabilization of Kruppel-like factor 4 protein in response to serum stimulation involves the ubiquitin-proteasome pathway. *Cancer Res* **65**, 10394-10400, doi:10.1158/0008-5472.CAN-05-2059 (2005).

40 Gamper, A. M. *et al.* Regulation of KLF4 turnover reveals an unexpected tissue-specific role of pVHL in tumorigenesis. *Mol Cell* **45**, 233-243, doi:10.1016/j.molcel.2011.11.031 (2012).

41 Alencar, G. F. *et al.* Stem Cell Pluripotency Genes Klf4 and Oct4 Regulate Complex SMC Phenotypic Changes Critical in Late-Stage Atherosclerotic Lesion Pathogenesis. *Circulation* **142**, 2045-2059, doi:10.1161/CIRCULATIONAHA.120.046672 (2020).

42 Libby, P. & Sasiela, W. Plaque stabilization: Can we turn theory into evidence? *Am J Cardiol* **98**, 26P-33P, doi:10.1016/j.amjcard.2006.09.017 (2006).

43 Brophy, M. L. *et al.* Myeloid-Specific Deletion of Epsins 1 and 2 Reduces Atherosclerosis by Preventing LRP-1 Downregulation. *Circ Res* **124**, e6-e19, doi:10.1161/CIRCRESAHA.118.313028 (2019).

44 Dhaliwal, N. K., Miri, K., Davidson, S., Tamim El Jarkass, H. & Mitchell, J. A. KLF4 Nuclear Export Requires ERK Activation and Initiates Exit from Naive Pluripotency. *Stem Cell Reports* **10**, 1308-1323, doi:10.1016/j.stemcr.2018.02.007 (2018).

45 Yap, C., Mieremet, A., de Vries, C. J. M., Micha, D. & de Waard, V. Six Shades of Vascular Smooth Muscle Cells Illuminated by KLF4 (Kruppel-Like Factor 4). *Arterioscler Thromb Vasc Biol* **41**, 2693-2707, doi:10.1161/ATVBAHA.121.316600 (2021).

46 Salmon, M. *et al.* KLF4 regulates abdominal aortic aneurysm morphology and deletion attenuates aneurysm formation. *Circulation* **128**, S163-174, doi:10.1161/CIRCULATIONAHA.112.000238 (2013).

47 Long, X., Bell, R. D., Gerthoffer, W. T., Zlokovic, B. V. & Miano, J. M. Myocardin is sufficient for a smooth muscle-like contractile phenotype. *Arterioscler Thromb Vasc Biol* **28**, 1505-1510, doi:10.1161/ATVBAHA.108.166066 (2008).

48 Deaton, R. A., Gan, Q. & Owens, G. K. Sp1-dependent activation of KLF4 is required for PDGF-BB-induced phenotypic modulation of smooth muscle. *Am J Physiol Heart Circ Physiol* **296**, H1027-1037, doi:10.1152/ajpheart.01230.2008 (2009).

49 Chattopadhyay, A. *et al.* Cholesterol-Induced Phenotypic Modulation of Smooth Muscle Cells to Macrophage/Fibroblast-like Cells Is Driven by an Unfolded Protein Response. *Arterioscler Thromb Vasc Biol* **41**, 302-316, doi:10.1161/ATVBAHA.120.315164 (2021).

50 Zhang, X. H., Zheng, B., Gu, C., Fu, J. R. & Wen, J. K. TGF-beta1 downregulates AT1 receptor expression via PKC-delta-mediated Sp1 dissociation from KLF4 and Smad-mediated PPAR-gamma association with KLF4. *Arterioscler Thromb Vasc Biol* **32**, 1015-1023,

doi:10.1161/ATVBAHA.111.244962 (2012).

51 Tsai, S. Y. *et al.* Oct4 and klf4 reprogram dermal papilla cells into induced pluripotent stem cells. *Stem Cells* **28**, 221-228, doi:10.1002/stem.281 (2010).

52 Kim, J. B. *et al.* Pluripotent stem cells induced from adult neural stem cells by reprogramming with two factors. *Nature* **454**, 646-650, doi:10.1038/nature07061 (2008).

53 Lee, S., Wottrich, S. & Bonavida, B. Crosstalks between Raf-kinase inhibitor protein and cancer stem cell transcription factors (Oct4, KLF4, Sox2, Nanog). *Tumour Biol* **39**, 1010428317692253, doi:10.1177/1010428317692253 (2017).

54 Cherepanova, O. A. *et al.* Activation of the pluripotency factor OCT4 in smooth muscle cells is atheroprotective. *Nat Med* **22**, 657-665, doi:10.1038/nm.4109 (2016).

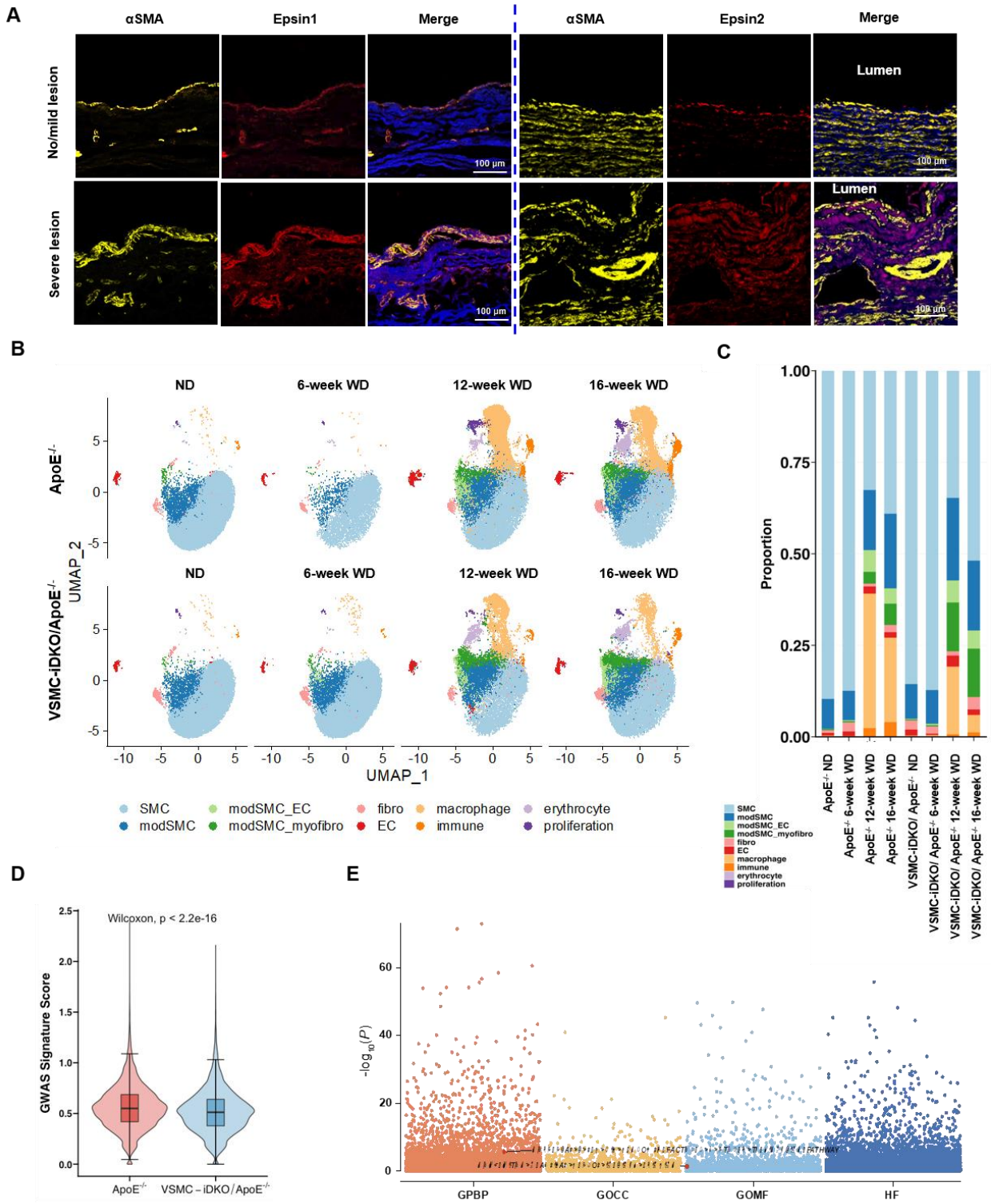
A
αSMA
Epsin1
Merge
αSMA
Epsin2
Merge
No/mild lesion
Severe lesion
Lumen
100 μm
B
ND
6-week WD
12-week WD
16-week WD
ApoE-/-
VSMC-iDKO/ApoE-/-
UMAP_2
UMAP_1
SMC
modSMC
modSMC_EC
modSMC_myofibro
fibro
EC
macrophage
immune
erythrocyte
proliferation
C
Proportion
ApoE-/- ND
ApoE-/- 6-week WD
ApoE-/- 12-week WD
ApoE-/- 16-week WD
VSMC-iDKO/ ApoE-/- ND
VSMC-iDKO/ ApoE-/- 6-week WD
VSMC-iDKO/ ApoE-/- 12-week WD
VSMC-iDKO/ ApoE-/- 16-week WD
D
Wilcoxon, p < 2.2e-16
GWAS Signature Score
ApoE-/-
VSMC – iDKO / ApoE-/-
E
-log10(P)
GPBP
GOCC
GOMF
HF

Fig 1. Human and mouse model of atherosclerosis for gene expression and scRNA profiling

A, Immuno-staining of epsin 1, epsin 2, αSMA and nuclei in human samples with no/mild or severe atherosclerotic lesion. Scale bar=100 μm.

B, UMAP plot showing the major cell types of mouse models across different diet feeding-week. Dots represent individual cells, and colors represent different cell populations.

C, Proportion of major cell types between *ApoE*$^{-/-}$ and VSMC-iDKO/*ApoE*$^{-/-}$ mice across different diet feeding-week.

D, Group comparison of GWAS CAD susceptibility signature mapped to scRNA-seq data between *ApoE*$^{-/-}$ and VSMC-iDKO/*ApoE*$^{-/-}$ mice with 16-week WD feeding. *P* value was calculated by Wilcoxon rank sum test.

E, Manhattan plot showing the differential biological GO pathways between *ApoE*$^{-/-}$ and VSMC-iDKO/*ApoE*$^{-/-}$ mice with 16-week WD feeding from scRNA-seq data. Each pathway was scored using *UCell* method deposited in *irGSEA* and *P* value was calculated by *t* test.

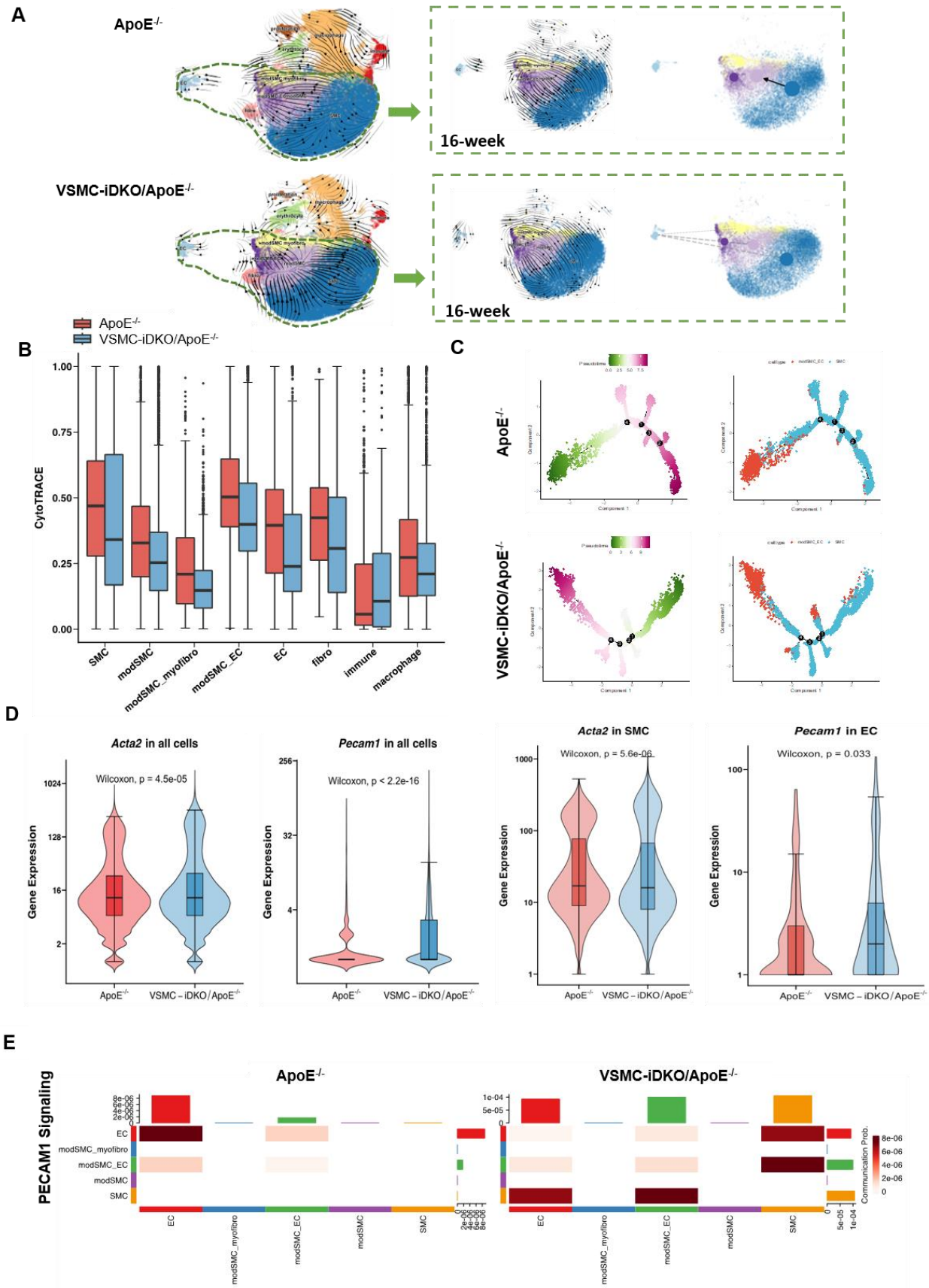
A
ApoE-/-
16-week
VSMC-iDKO/ApoE-/-
16-week
ApoE-/-
VSMC-iDKO/ApoE-/-
B
CytoTRACE
SMC
modSMC
modSMC_myofibro
modSMC_EC
EC
fibro
immune
macrophage
C
ApoE-/-
VSMC-iDKO/ApoE-/-
D
Acta2 in all cells
Wilcoxon, p = 4.5e-05
Pecam1 in all cells
Wilcoxon, p < 2.2e-16
Acta2 in SMC
Wilcoxon, p = 5.6e-06
Pecam1 in EC
Wilcoxon, p = 0.033
Gene Expression
ApoE-/-
VSMC – iDKO/ApoE-/-
E
PECAM1 Signaling
ApoE-/-
VSMC-iDKO/ApoE-/-
Communication Prob.

Fig 2. VSMC phenotypic transitions based on scRNA data.

A, UMAP visualization of RNA velocity recapitulating SMC phenotypic modulation for individual cells of mouse models, the expanded for 16-week WD feeding groups using *scVelo* package.

B, Boxplot showing differential inferred CytoTRACE scores of major cell types between *ApoE*$^{-/-}$ and VSMC-iDKO/*ApoE*$^{-/-}$ mice.

C, The trajectory path from SMC to modSMC_EC cells between *ApoE*$^{-/-}$ and VSMC-iDKO/*ApoE*$^{-/-}$ mice inferred by *Monocle2*. Each dot represents a single cell. The trajectory direction is determined by the predicted pseudotime. The trajectories were colored by pseudotime (left) and cluster identities (right).

D, Differential gene expression of canonical markers of SMC (*Acta2*) and EC (*Pecam1*) cells between *ApoE*$^{-/-}$ and VSMC-iDKO/*ApoE*$^{-/-}$ mice. *P* value was calculated by Wilcoxon rank sum test.

E, Heatmap of PECAM1 signaling across SMC phenotypic modulation between *ApoE*$^{-/-}$ and VSMC-iDKO/*ApoE*$^{-/-}$ mice. PECAM1 signaling was calculated using *CellChat* package.

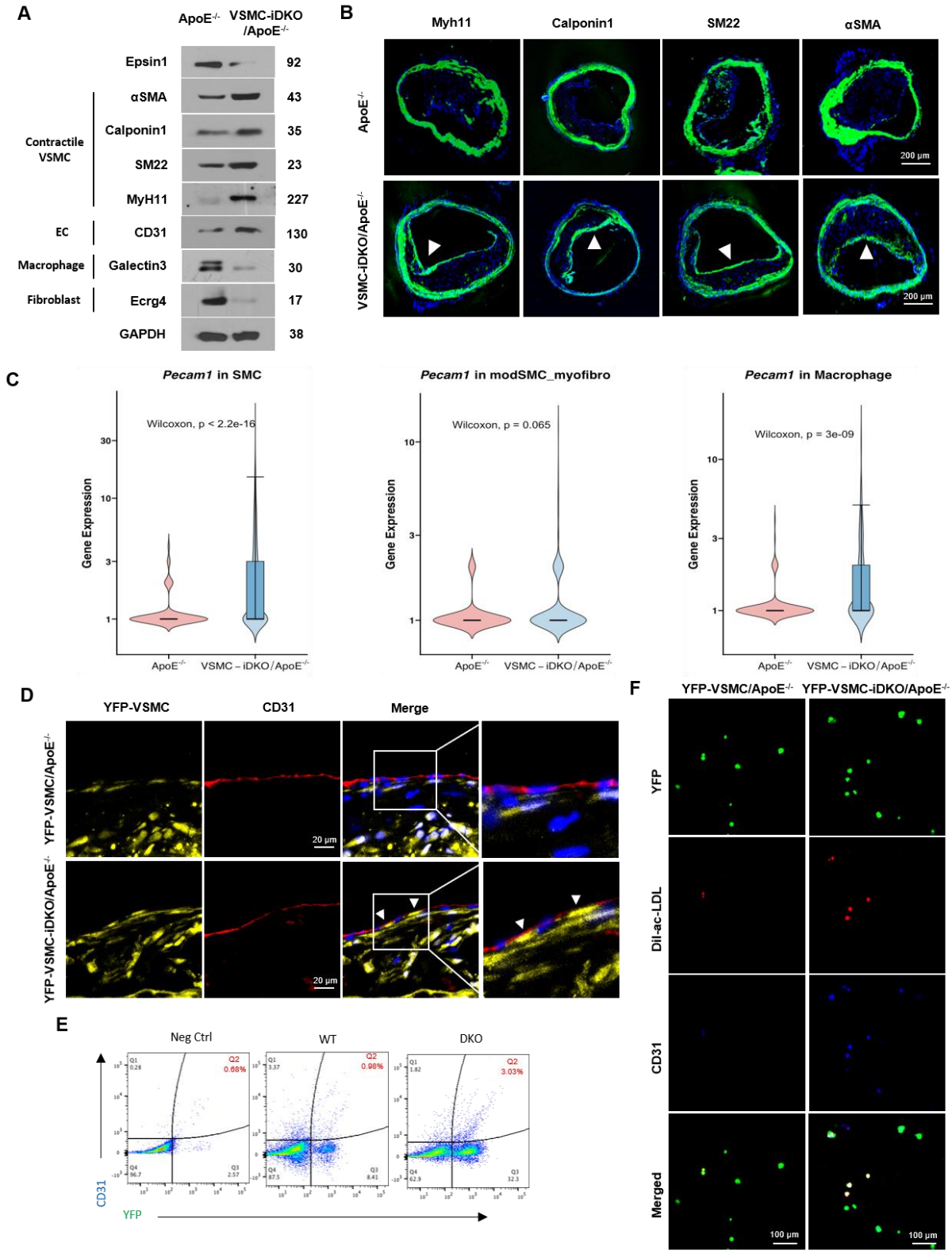
A
ApoE-/-
VSMC-iDKO /ApoE-/-
Epsin1
αSMA
Calponin1
SM22
MyH11
CD31
Galectin3
Ecrg4
GAPDH
Contractile VSMC
EC
Macrophage
Fibroblast
92
43
35
23
227
130
30
17
38
B
Myh11
Calponin1
SM22
αSMA
ApoE-/-
VSMC-iDKO/ApoE-/-
200 μm
C
Pecam1 in SMC
Wilcoxon, p < 2.2e-16
Pecam1 in modSMC_myofibro
Wilcoxon, p = 0.065
Pecam1 in Macrophage
Wilcoxon, p = 3e-09
Gene Expression
ApoE-/-
VSMC – iDKO/ApoE-/-
D
YFP-VSMC
CD31
Merge
YFP-VSMC/ApoE-/-
YFP-VSMC-iDKO/ApoE-/-
20 μm
E
Neg Ctrl
WT
DKO
Q2 0.68%
Q2 0.98%
Q2 3.03%
CD31
YFP
F
YFP-VSMC/ApoE-/-
YFP-VSMC-iDKO/ApoE-/-
YFP
DiI-ac-LDL
CD31
Merged
100 μm

Fig 3. VSMC contractile markers and VSMC-drived ECs was reduced by epsins during atherosclerosis.

A, The protein expressions of VSMC differentiation markers, EC marker CD31, macrophages marker Galectin3 and fibroblast marker Ecrg4 were measured in aortas of *ApoE*$^{-/-}$ and VSMC-iDKO/*ApoE*$^{-/-}$ mice fed a WD for 20 weeks.

B, Immuno-staining of αSMA, SM22, Calponin1 and MyH11 in truncus brachiocephalicus of *ApoE*$^{-/-}$ and VSMC-iDKO/*ApoE*$^{-/-}$mice fed a WD for 20 weeks.

C, Differential gene expression of *Pecam1* between *ApoE*$^{-/-}$ and VSMC-iDKO/*ApoE*$^{-/-}$ mice across cell types from scRNA-seq data. *P* value was calculated by Wilcoxon rank sum test.

D, Immuno-staining of EC marker CD31 in truncus brachiocephalicus of SMC-lineage tracing mice to confirm VSMC transition to endothelial-like cells reduced by epsins during atherosclerosis. Scale bar=20 μm.

E, The number of cells with CD31+ and their corresponding control in YFP-tagged cells by flow cytometry analysis.

F, Dil-ac-LDL uptake assays followed by immuno-staining of EC marker CD31 in sorted YFP-tagged cells to show the EC function of VSMCs-drived EC-like cells. Scale bar=100 μm.

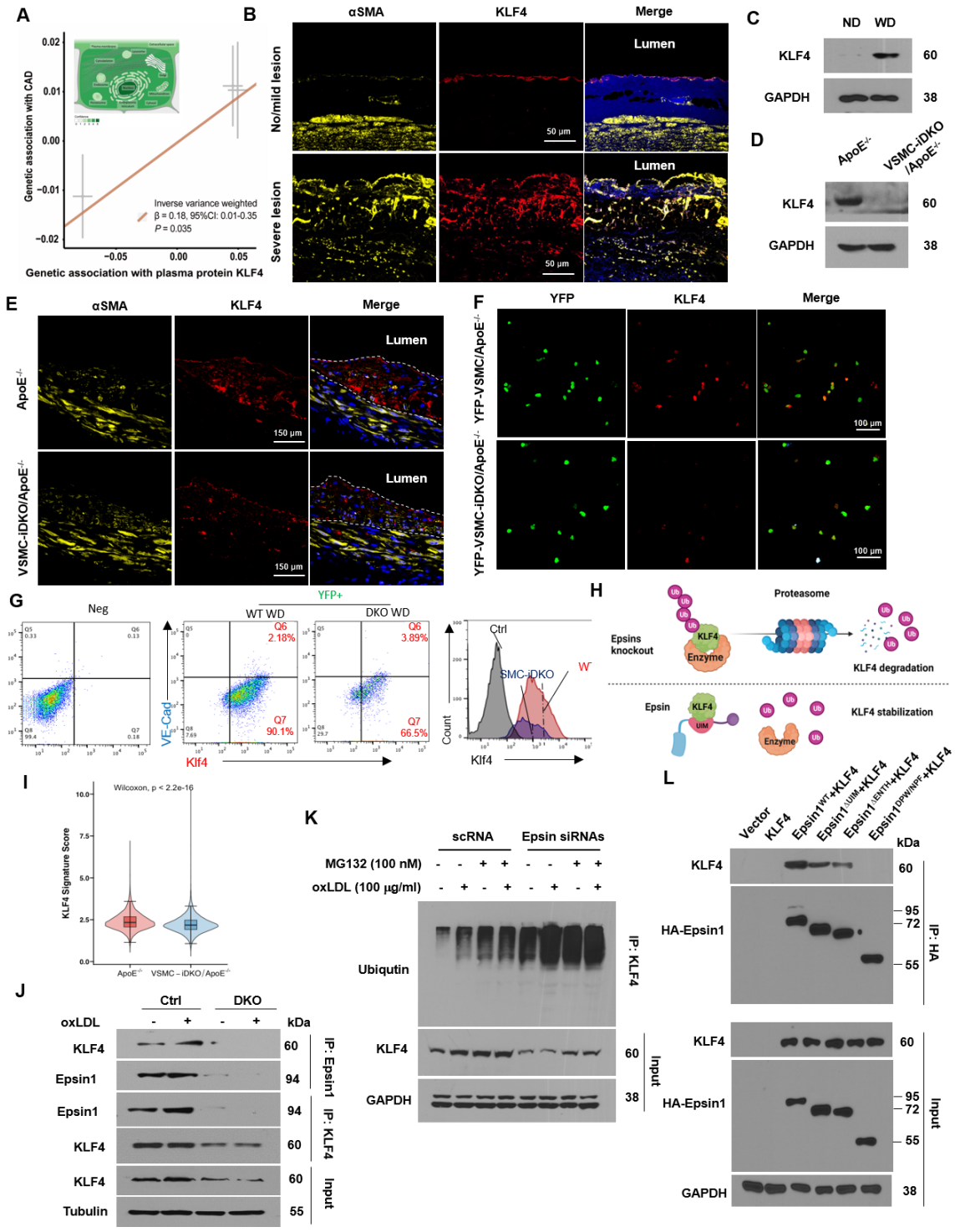
A
Genetic association with CAD
Genetic association with plasma protein KLF4
Inverse variance weighted
β = 0.18, 95%CI: 0.01-0.35
P = 0.035
B
αSMA
KLF4
Merge
No/mild lesion
Severe lesion
Lumen
50 μm
C
ND
WD
KLF4
GAPDH
60
38
D
ApoE-/-
VSMC-iDKO /ApoE-/-
KLF4
GAPDH
60
38
E
αSMA
KLF4
Merge
ApoE-/-
VSMC-iDKO/ApoE-/-
Lumen
150 μm
F
YFP
KLF4
Merge
YFP-VSMC/ApoE-/-
YFP-VSMC-iDKO/ApoE-/-
100 μm
G
Neg
YFP+
WT WD
DKO WD
Q6 2.18%
Q7 90.1%
Q6 3.89%
Q7 66.5%
VE-Cad
Klf4
Ctrl
SMC-iDKO
Count
H
Proteasome
Epsins knockout
KLF4
Enzyme
Ub
KLF4 degradation
Epsin
UIM
KLF4 stabilization
I
Wilcoxon, p < 2.2e-16
KLF4 Signature Score
ApoE-/-
VSMC – iDKO / ApoE-/-
J
Ctrl
DKO
oxLDL
kDa
KLF4
Epsin1
Tubulin
60
94
55
IP: Epsin1
IP: KLF4
Input
K
scRNA
Epsin siRNAs
MG132 (100 nM)
oxLDL (100 μg/ml)
Ubiqutin
KLF4
GAPDH
60
38
IP: KLF4
Input
L
Vector
KLF4
Epsin1WT+KLF4
Epsin1ΔUIM+KLF4
Epsin1ΔENTH+KLF4
Epsin1DPW/NPF+KLF4
kDa
HA-Epsin1
95
72
55
IP: HA
Input

Fig 4. Epsins upregulated the Expression of KLF4 by Suppressing KLF4 ubiquitination.

A, Scatter plots for Mendelian Randomization analysis of putative causal association between plasma KLF4 protein and CAD risk. *P* value was calculated with IVW regression using *TwoSampleMR* package. Subcellular location of KLF4 was derived from GeneCards (https://www.genecards.org/cgi-bin/carddisp.pl?gene=KLF4#localization)

B, Immuno-staining of KLF4, αSMA and nuclei in human samples with no/mild or severe atherosclerotic lesion. Scale bar=50 μm.

C-D, Immuno-blot analysis of KLF4 expression in aortas from ApoE$^{-/-}$ mice fed a ND or WD (**C**) and ApoE$^{-/-}$ and VSMC-iDKO/ApoE$^{-/-}$ mice fed a WD for 20 weeks (**D**).

E, Immuno-staining of KLF4 in truncus brachiocephalicus of SMC-lineage tracing mice fed a WD for 20 weeks. Scale bar=150 μm.

F, KLF4 expression in sorted YFP-tagged cells under confocal microscope. Scale bar=100 μm.

G, The number of cells with VE-Cadherin+ and KLF4+ in YFP-tagged cells by flow cytometry analysis.

H, Proposed model of the mechanism. Epsins promoted the stability of KLF4 and hindered KLF4 ubiquitination via binding to KLF4 with UIM and ENTH domain.

I, Differential signature score of KLF4 binding genes between *ApoE*$^{-/-}$ and VSMC-iDKO/*ApoE*$^{-/-}$ mice from scRNA-seq data. *P* value was calculated by Wilcoxon rank sum test. The signature score was calculated using differential 1113 target genes of KLF4 binding site with *PercentageFeatureSet* function deposited in *Seurat* package.

J, The interaction between epsin and KLF4 in primary VSMCs from ApoE$^{-/-}$ and VSMC-iDKO/ApoE$^{-/-}$ mice treated with 100 μM oxLDL was tested with immunoprecipitation and analyzed with western blot.

K, The KLF4 ubiquitin level in VSMCs transfected with scRNA or epsin 1/2 siRNAs followed by 100 nM MG132 and 100 μM oxLDL treatment was measured by immunoprecipitation and blotting.

L, HA-tagged epsin 1 or epsin 1 domains were co-transfected with pCX4-KLF4 into HEK 293T cells, after 24 hrs, cell lysis was immunoprecipitated with HA antibody, followed by western blot with KLF4 and HA antibodies.

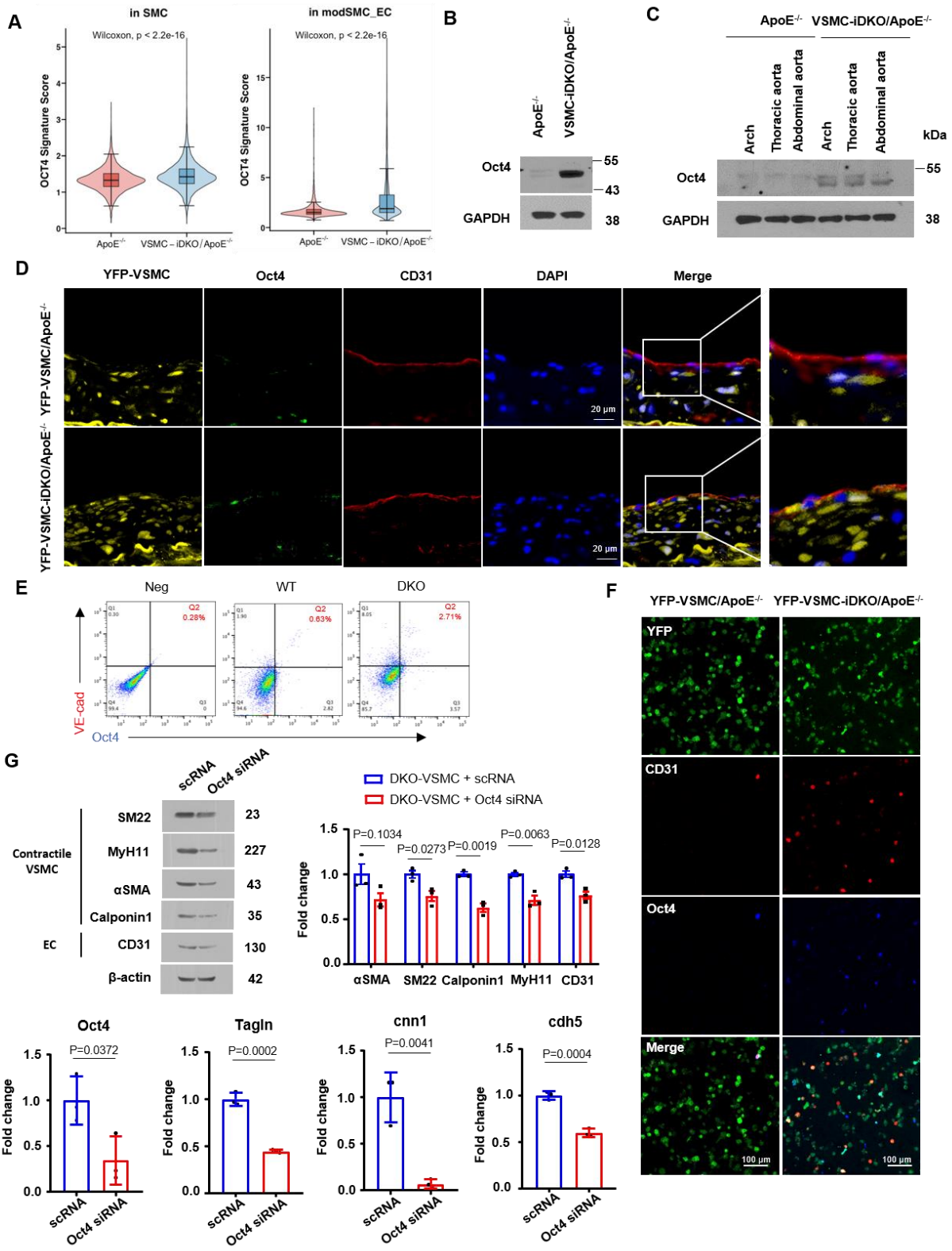
A
in SMC
Wilcoxon, p < 2.2e-16
OCT4 Signature Score
ApoE-/-
VSMC – iDKO / ApoE-/-
in modSMC_EC
Wilcoxon, p < 2.2e-16
B
ApoE-/-
VSMC-iDKO/ApoE-/-
Oct4
GAPDH
55
43
38
C
ApoE-/-
VSMC-iDKO/ApoE-/-
Arch
Thoracic aorta
Abdominal aorta
kDa
Oct4
GAPDH
55
38
D
YFP-VSMC
Oct4
CD31
DAPI
Merge
YFP-VSMC/ApoE-/-
YFP-VSMC-iDKO/ApoE-/-
20 μm
E
Neg
WT
DKO
Q2 0.28%
Q2 0.63%
Q2 2.71%
VE-cad
Oct4
F
YFP-VSMC/ApoE-/-
YFP-VSMC-iDKO/ApoE-/-
YFP
CD31
Oct4
Merge
100 μm
G
scRNA
Oct4 siRNA
Contractile VSMC
EC
SM22
MyH11
αSMA
Calponin1
CD31
β-actin
23
227
43
35
130
42
DKO-VSMC + scRNA
DKO-VSMC + Oct4 siRNA
Fold change
P=0.1034
P=0.0273
P=0.0019
P=0.0063
P=0.0128
αSMA
SM22
Calponin1
MyH11
CD31
H
Oct4
P=0.0372
Tagln
P=0.0002
cnn1
P=0.0041
cdh5
P=0.0004
Fold change
scRNA
Oct4 siRNA

Fig 5. VSMC-specific Epsins Deficiency Promoted the Expression of EC Markers in VSMCs via Augmenting the Oct4 Expression in Atherosclerotic Plaques

A, Differential signature score of OCT4 binding genes between *ApoE*$^{-/-}$ and VSMC-iDKO/*ApoE*$^{-/-}$ mice across cells types derived from scRNA-seq data. *P* value was calculated by Wilcoxon rank sum test. The signature score was calculated using differential 898 target genes of OCT4 binding site with *PercentageFeatureSet* function deposited in *Seurat* package.

B-C, Immuno-blot analysis of Oct4 expression in whole aortas and different part of aortas of ApoE$^{-/-}$ and VSMC-iDKO/ApoE$^{-/-}$ mice fed a WD for 20 weeks and normalized to the expression of GAPDH.

D, Immuno-staining of Oct4 in truncus brachiocephalicus of SMC-lineage tracing mice with 14-week WD. Scale bar=20 μm.

E, The number of cells with VE-Cadherin+ and Oct4+ in YFP-tagged cells by flow cytometry analysis.

F, The localization of Oct4 and CD31 expression in sorted YFP-tagged cells under confocal microscope. Scale bar=100 μm.

G-H, The protein and mRNA expressions of VSMC differentiation markers and EC markers were measured in long term cultured VSMCs from VSMC-iDKO/ApoE$^{-/-}$ mice transfected with scramble siRNA (scRNA) or Oct4 siRNA for 48 hrs and quantitation (n=3).

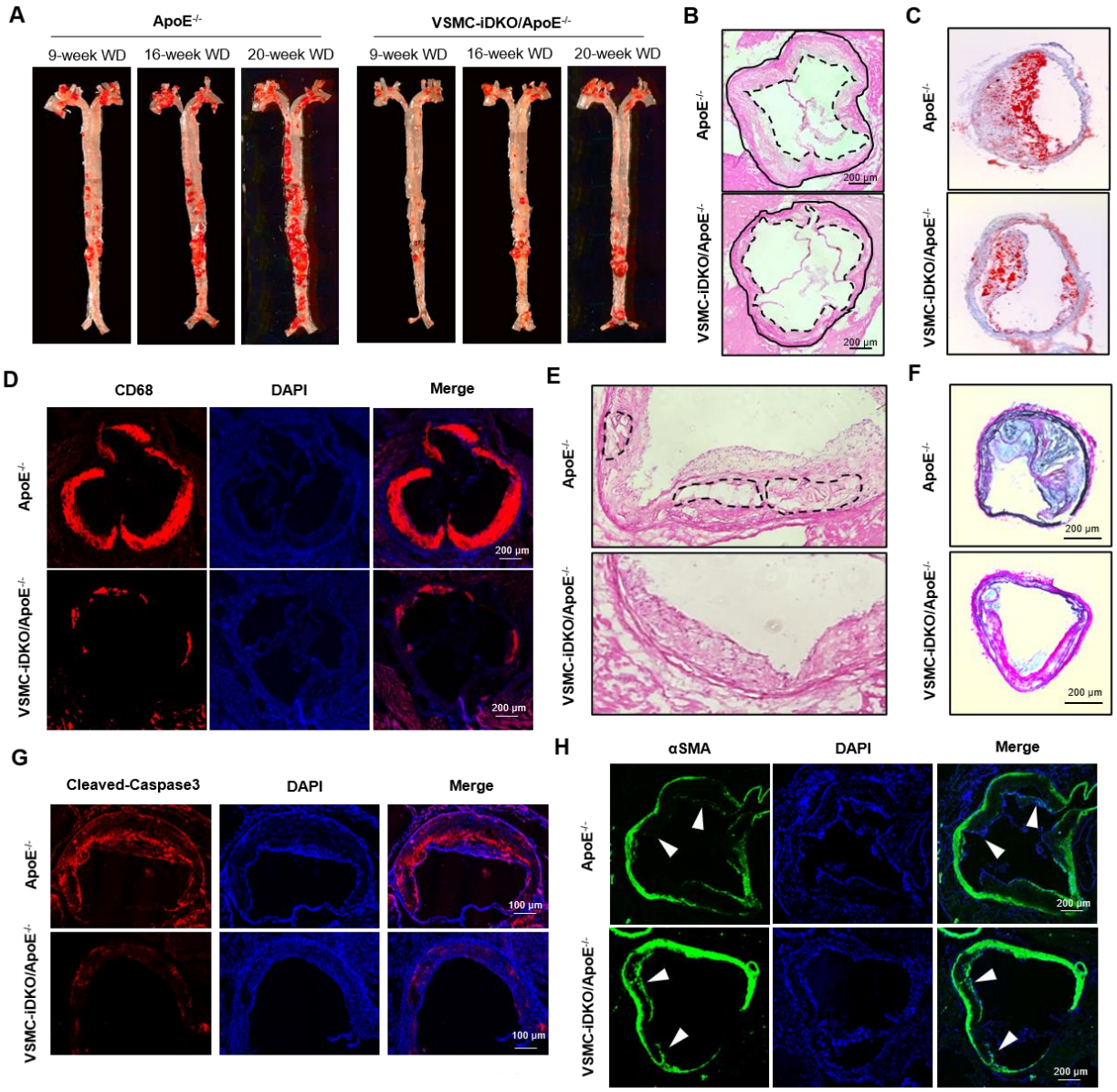
A
ApoE-/-
VSMC-iDKO/ApoE-/-
9-week WD
16-week WD
20-week WD
9-week WD
16-week WD
20-week WD
B
ApoE-/-
VSMC-iDKO/ApoE-/-
200 μm
200 μm
C
ApoE-/-
VSMC-iDKO/ApoE-/-
D
CD68
DAPI
Merge
ApoE-/-
VSMC-iDKO/ApoE-/-
200 μm
200 μm
E
ApoE-/-
VSMC-iDKO/ApoE-/-
F
ApoE-/-
VSMC-iDKO/ApoE-/-
200 μm
200 μm
G
Cleaved-Caspase3
DAPI
Merge
ApoE-/-
VSMC-iDKO/ApoE-/-
100 μm
100 μm
H
αSMA
DAPI
Merge
ApoE-/-
VSMC-iDKO/ApoE-/-
200 μm
200 μm

Fig 6. VSMC-specific Epsin 1 and 2 Deficiency Reduces Atherosclerotic Plaques and Enhanced the Stability of lesionin mice. ApoE$^{-/-}$ and VSMC-iDKO/ApoE$^{-/-}$ mice were fed a Western Diet (WD) for 9, 16 and 20 weeks. The sections of aortic root and truncus brachiocephalicus were collected from the ApoE$^{-/-}$ and VSMC-iDKO/ApoE$^{-/-}$ mice fed a WD for 20 weeks.

A, *En face* Oil Red O (ORO) staining of the whole aortas from ApoE$^{-/-}$ or VSMC-iDKO/ApoE$^{-/-}$ mice fed a Western Diet (WD) for 9, 16 and 20 weeks.

B, hematoxylin-eosin(H&E) staining of aortic roots showed the size of atherosclerotic lesion.

C, ORO staining of truncus brachiocephalicus were used to show the lipid accumulation in the lesion.

D, Immuno-staining of CD68 in aortic roots were performed to show the inflammation in lesion. Scale bar=200 μm.

E, H&E staining of aortic roots. Necrotic cores were marked.

F, Verhoeff–Van Gieson's staining of truncus brachiocephalicus were performed to show the stability of the lesion.

G-H, Immuno-staining of cleaved-caspase3 (**H**) and αSMA (**I**) in aortic roots to show the apoptosis cells in the plaques. Quantitation of data (n=6). Scale bar=200 μm.

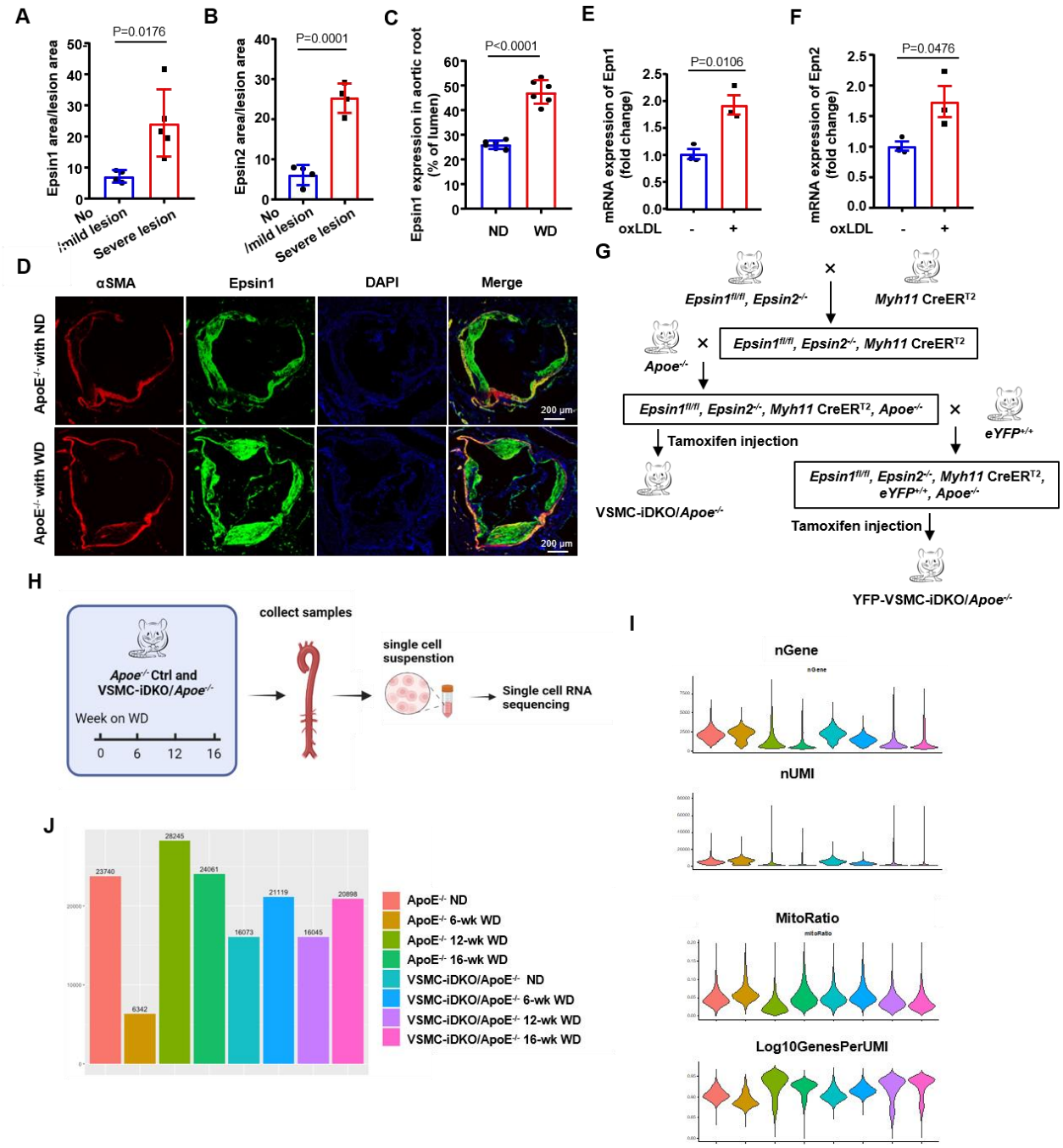
A
P=0.0176
Epsin1 area/lesion area
No
Mild lesion
Severe lesion
B
P=0.0001
Epsin2 area/lesion area
C
P<0.0001
Epsin1 expression in aortic root (% of lumen)
ND
WD
E
P=0.0106
mRNA expression of Epn1 (fold change)
oxLDL
F
P=0.0476
mRNA expression of Epn2 (fold change)
D
αSMA
Epsin1
DAPI
Merge
ApoE-/- with ND
ApoE-/- with WD
200 μm
G
Epsin1fl/fl, Epsin2-/-
Myh11 CreERT2
Epsin1fl/fl, Epsin2-/-, Myh11 CreERT2
Apoe-/-
Epsin1fl/fl, Epsin2-/-, Myh11 CreERT2, Apoe-/-
eYFP+/+
Tamoxifen injection
VSMC-iDKO/Apoe-/-
Epsin1fl/fl, Epsin2-/-, Myh11 CreERT2, eYFP+/+, Apoe-/-
YFP-VSMC-iDKO/Apoe-/-
H
Apoe-/- Ctrl and VSMC-iDKO/Apoe-/-
Week on WD
0
6
12
16
collect samples
single cell suspenstion
Single cell RNA sequencing
I
nGene
nUMI
MitoRatio
Log10GenesPerUMI
J
23740
6342
28245
24061
16073
21119
16045
20898
ApoE-/- ND
ApoE-/- 6-wk WD
ApoE-/- 12-wk WD
ApoE-/- 16-wk WD
VSMC-iDKO/ApoE-/- ND
VSMC-iDKO/ApoE-/- 6-wk WD
VSMC-iDKO/ApoE-/- 12-wk WD
VSMC-iDKO/ApoE-/- 16-wk WD

Supplemental Fig 1. Human and mouse model of atherosclerosis for gene expression and scRNA profiling

A-B, Quantitation of epsin 1, epsin 2 expression in human samples (n=4-5).

C-D, Increase mRNA levels in epsins 1 and 2 in response to a 12 hrs exposure to 100 μg/ml oxLDL (n=3).

E-F, Immuno-staining of epsin 1 and αSMA in *ApoE*$^{-/-}$ mice fed a normal diet (ND) or Western Diet (WD). Scale bar=200 μm. Quantitation of data (n=6).

G-H, Mouse model construction (**G**) and corresponding scRNA-seq experimental workflow (**H**).

I, Violin plot showing the quality of mouse model scRNA-seq data, colored by different diet feeding-week.

J, Barplot showing available cells from mouse models across different diet feeding-week.

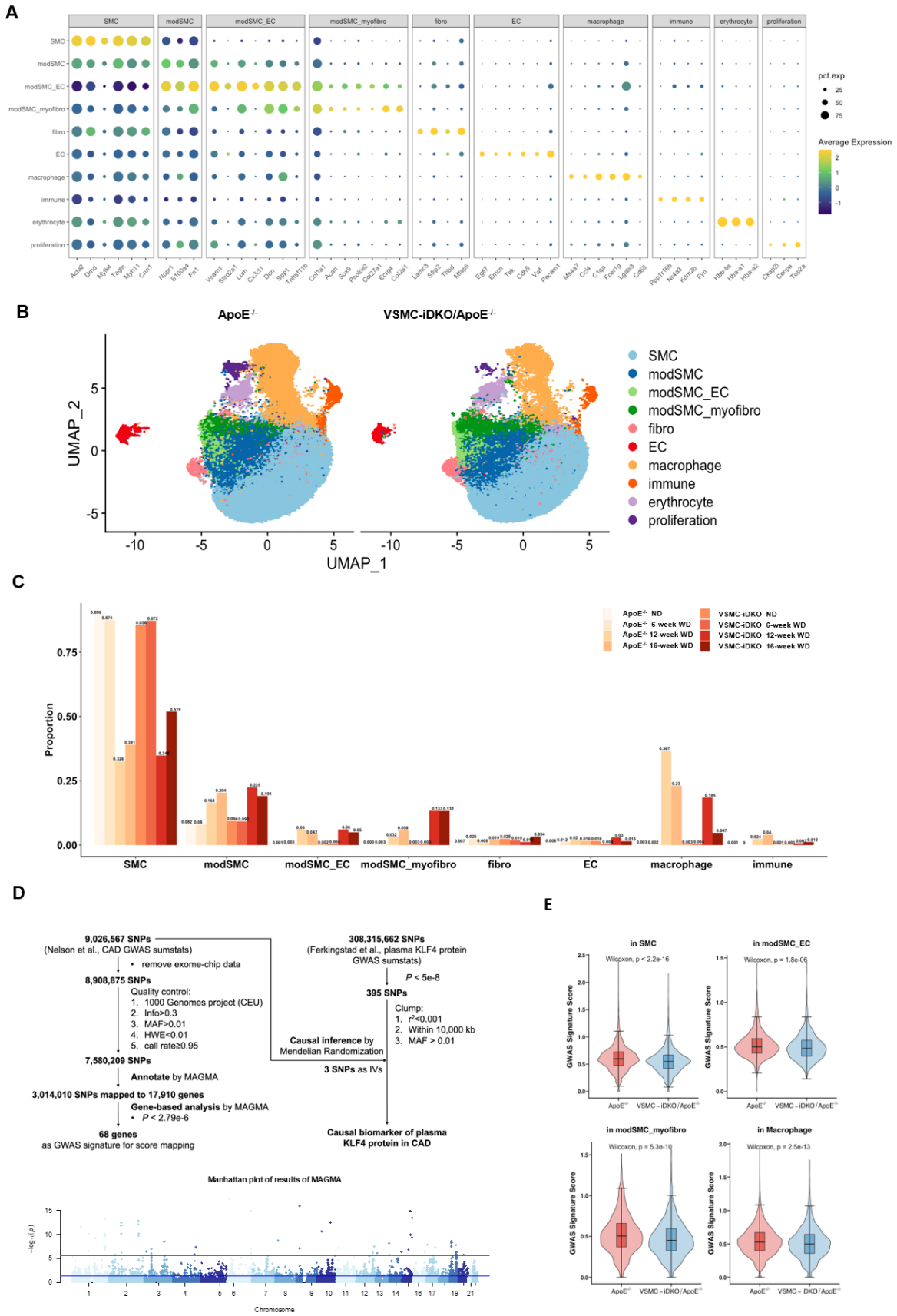
A
SMC
modSMC
modSMC_EC
modSMC_myofibro
fibro
EC
macrophage
immune
erythrocyte
proliferation
pct.exp
Average Expression
B
ApoE-/-
VSMC-iDKO/ApoE-/-
UMAP_1
UMAP_2
SMC
modSMC
modSMC_EC
modSMC_myofibro
fibro
EC
macrophage
immune
erythrocyte
proliferation
C
Proportion
ApoE-/- ND
ApoE-/- 6-week WD
ApoE-/- 12-week WD
ApoE-/- 16-week WD
VSMC-iDKO ND
VSMC-iDKO 6-week WD
VSMC-iDKO 12-week WD
VSMC-iDKO 16-week WD
D
9,026,567 SNPs
(Nelson et al., CAD GWAS sumstats)
remove exome-chip data
8,908,875 SNPs
Quality control:
1. 1000 Genomes project (CEU)
2. Info>0.3
3. MAF>0.01
4. HWE<0.01
5. call rate≥0.95
7,580,209 SNPs
Annotate by MAGMA
3,014,010 SNPs mapped to 17,910 genes
Gene-based analysis by MAGMA
P < 2.79e-6
68 genes
as GWAS signature for score mapping
308,315,662 SNPs
(Ferkingstad et al., plasma KLF4 protein GWAS sumstats)
P < 5e-8
395 SNPs
Clump:
1. r2<0.001
2. Within 10,000 kb
3. MAF > 0.01
Causal inference by Mendelian Randomization
3 SNPs as IVs
Causal biomarker of plasma KLF4 protein in CAD
Manhattan plot of results of MAGMA
Chromosome
E
in SMC
Wilcoxon, p < 2.2e-16
in modSMC_EC
Wilcoxon, p = 1.8e-06
in modSMC_myofibro
Wilcoxon, p = 5.3e-10
in Macrophage
Wilcoxon, p = 2.5e-13
GWAS Signature Score
ApoE-/-
VSMC-iDKO/ApoE-/-

Supplemental Fig 2. scRNA profiling of atherosclerotic mouse model and CAD GWAS of general population

A, Dot heatmap showing the expression of typical marker genes for major cell types in mouse models.

B, UMAP visualization of major cell types across each mouse model, colored by cell types.

C, Barplot showing the proportion of major cell types derived from mouse models across different diet feeding-week.

D, Flowchart of the identification of CAD susceptibility genes and the causal inference of plasma KLF4 on CAD risk. Manhattan plot showing the genome-wide susceptibility genes of CAD using MAGMA. The red line represents the genome-wide significance at $P<0.05/17910$.

E, Differential signature score of GWAS genes between *ApoE*$^{-/-}$ and VSMC-iDKO/*ApoE*$^{-/-}$ mice across candidate cell types from scRNA-seq data. *P* value was calculated by Wilcoxon rank sum test. The signature score was calculated using 68 CAD susceptibility genes.

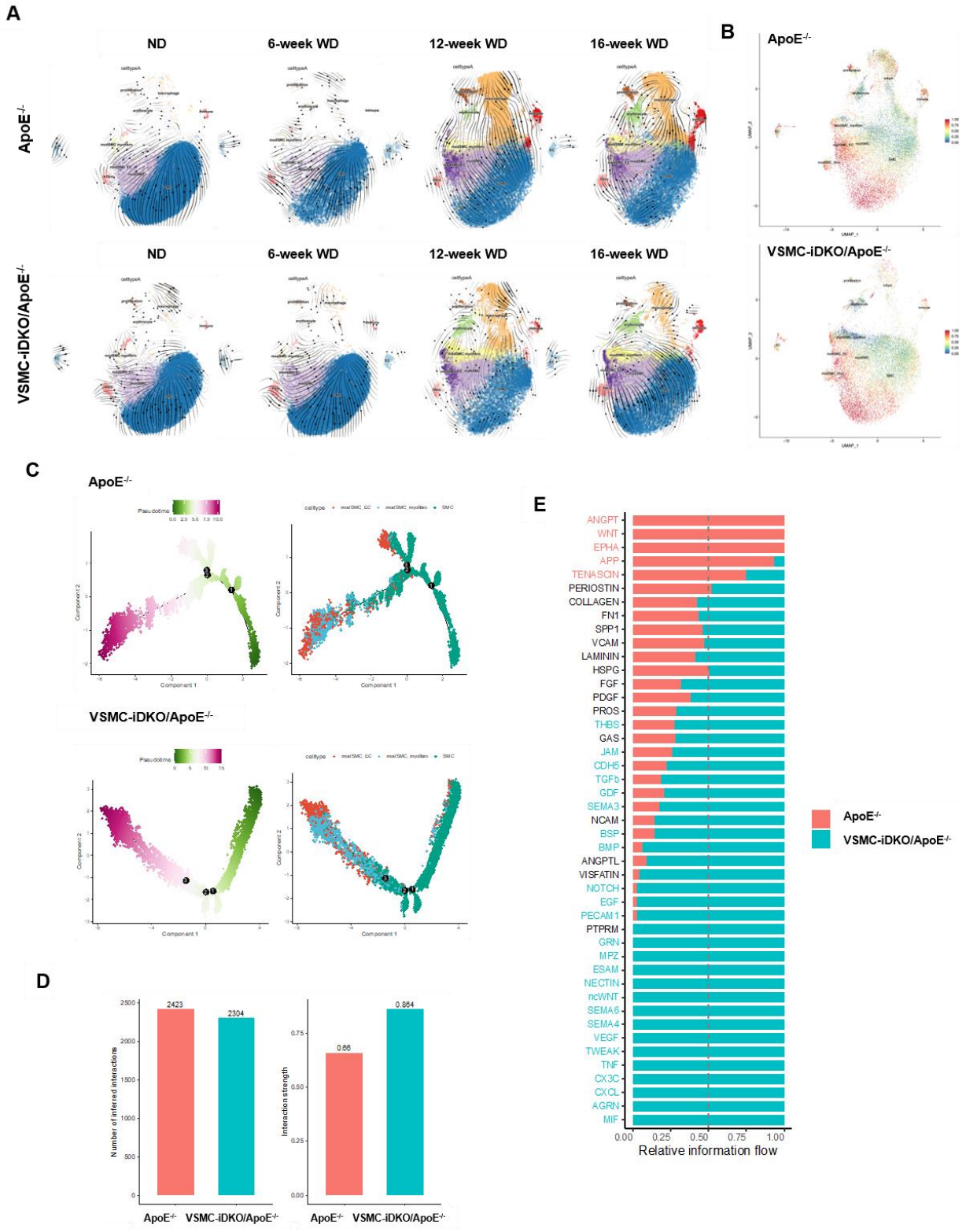
A
ND
6-week WD
12-week WD
16-week WD
ApoE-/-
VSMC-iDKO/ApoE-/-
B
ApoE-/-
VSMC-iDKO/ApoE-/-
C
ApoE-/-
VSMC-iDKO/ApoE-/-
Pseudotime
celltype
Component 1
Component 2
D
Number of inferred interactions
Interaction strength
2423
2304
0.86
0.864
ApoE-/-
VSMC-iDKO/ApoE-/-
E
ANGPT
WNT
EPHA
APP
TENASCIN
PERIOSTIN
COLLAGEN
FN1
SPP1
VCAM
LAMININ
HSPG
FGF
PDGF
PROS
THBS
GAS
JAM
CDH5
TGFb
GDF
SEMA3
NCAM
BSP
BMP
ANGPTL
VISFATIN
NOTCH
EGF
PECAM1
PTPRM
GRN
MPZ
ESAM
NECTIN
ncWNT
SEMA6
SEMA4
VEGF
TWEAK
TNF
CX3C
CXCL
AGRN
MIF
Relative information flow
ApoE-/-
VSMC-iDKO/ApoE-/-

Supplemental Fig 3. VSMC phenotypic transitions based on scRNA data.

A, UMAP visualization of inferred RNA velocity for individual cells of mouse models across different diet feeding-week.

B, UMAP visualization of inferred CytoTRACE scores for major cell types between *ApoE*$^{-/-}$ and VSMC-iDKO/*ApoE*$^{-/-}$ mice.

C, The trajectory path of SMC phenotypic modulation clusters between *ApoE*$^{-/-}$ and VSMC-iDKO/*ApoE*$^{-/-}$ mice inferred by Monocle2. Each dot represents a single cell. The trajectory direction is determined by the predicted pseudotime. The trajectories were colored by pseudotime (left) and cluster identities (right).

D, Global summary of number and strength of all interactions in *ApoE*$^{-/-}$ and VSMC-iDKO/*ApoE*$^{-/-}$ mice.

E, SMC transition relevant signaling pathways enhanced and suppressed with DKO treatment, identified using *CellChat* package.

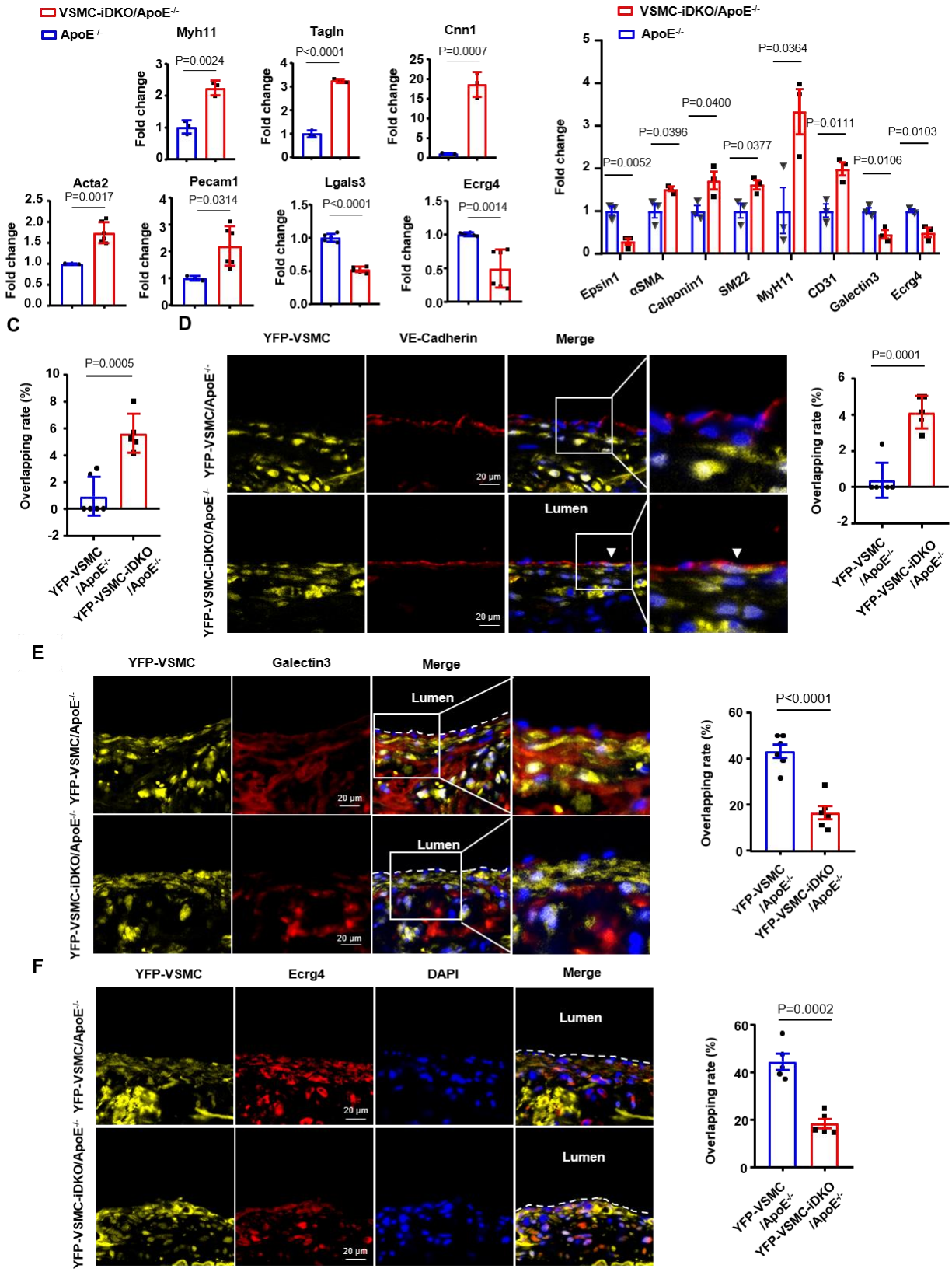
VSMC-iDKO/ApoE-/-
ApoE-/-
Myh11
P=0.0024
Tagln
P<0.0001
Cnn1
P=0.0007
Acta2
P=0.0017
Pecam1
P=0.0314
Lgals3
P<0.0001
Ecrg4
P=0.0014
Fold change
C
D
Epsin1
αSMA
Calponin1
SM22
MyH11
CD31
Galectin3
Ecrg4
P=0.0052
P=0.0396
P=0.0400
P=0.0377
P=0.0364
P=0.0111
P=0.0106
P=0.0103
YFP-VSMC
VE-Cadherin
Merge
YFP-VSMC/ApoE-/-
YFP-VSMC-iDKO/ApoE-/-
Lumen
20 μm
Overlapping rate (%)
P=0.0005
P=0.0001
YFP-VSMC /ApoE-/-
YFP-VSMC-iDKO /ApoE-/-
E
Galectin3
P<0.0001
F
DAPI
P=0.0002

Supplemental Fig 4. VSMC differentiation markers was regulated by epsins during atherosclerosis.

A, The mRNA expressions of VSMC marker genes, EC marker *Pecam1*, macrophage marker *lgals3* and fibroblast marker *Ecrg4* were measured in aortas of *ApoE*$^{-/-}$ and VSMC-iDKO/*ApoE*$^{-/-}$ mice fed a WD for 20 weeks, normalized to the actin.

B, Quantitation of western blot analysis of protein expressions of VSMC, EC, macrophage and fibroblast markers and normalized to the expression of GAPDH (n=3).

C, Quantitation of data of the immunostaining of EC marker CD31 in truncus brachiocephalicus of SMC-lineage tracing mice (n=5-6).

D-F, Immuno-staining of EC marker VE-Cadherin (**D**), macrophage marker Galectin3 (**E**) and fibroblast marker Ecrg4 (**F**) in truncus brachiocephalicus of SMC-lineage tracing mice to confirm VSMC transition to endothelial-like cells reduced by epsins during atherosclerosis. Scale bar=20 μm. Quantitation of data (n=5-6).

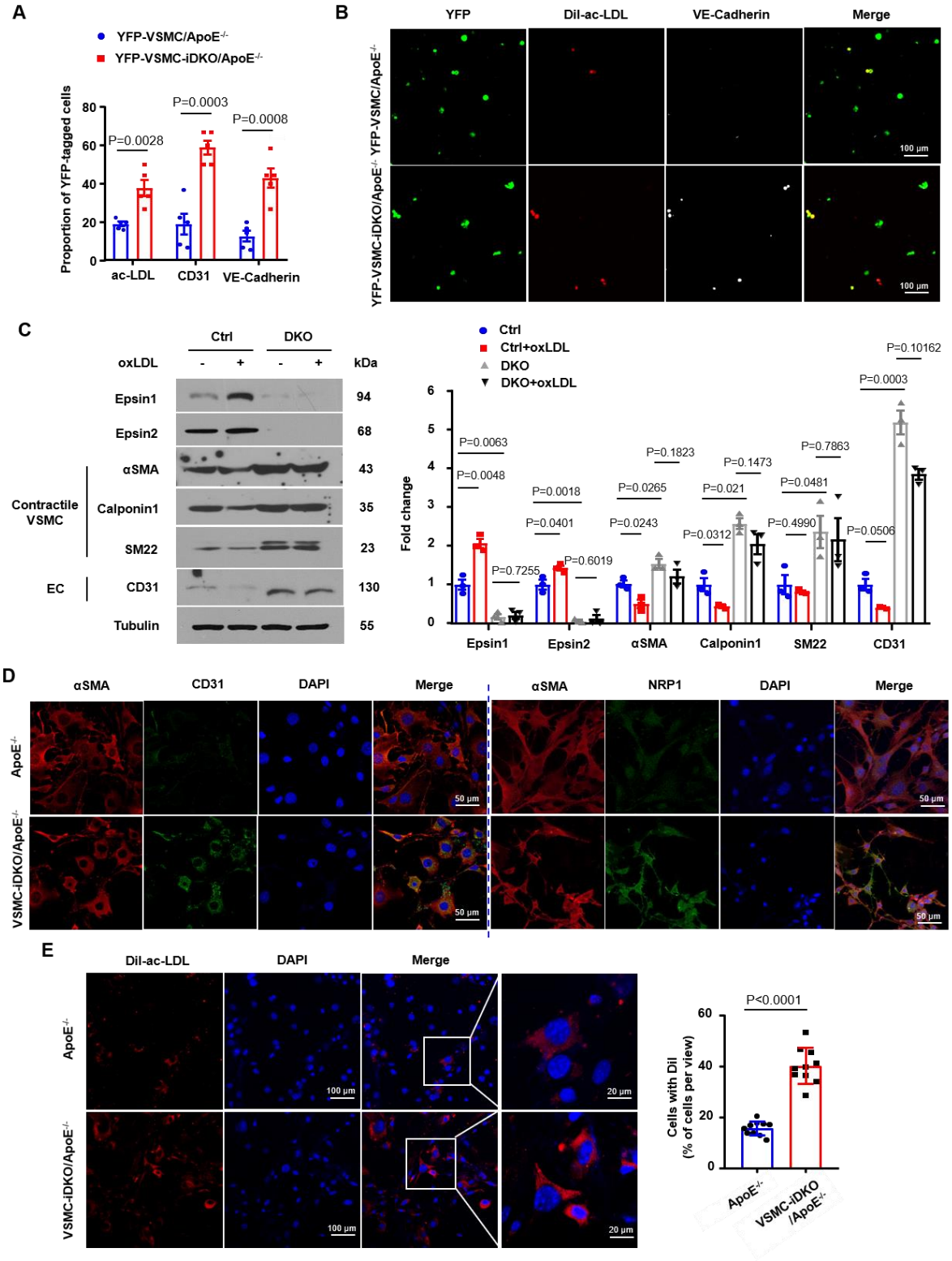
A
YFP-VSMC/ApoE-/-
YFP-VSMC-iDKO/ApoE-/-
Proportion of YFP-tagged cells
P=0.0028
P=0.0003
P=0.0008
ac-LDL
CD31
VE-Cadherin
B
YFP
DiI-ac-LDL
VE-Cadherin
Merge
YFP-VSMC/ApoE-/-
YFP-VSMC-iDKO/ApoE-/-
100 μm
C
Ctrl
DKO
oxLDL
kDa
Epsin1
Epsin2
αSMA
Calponin1
SM22
CD31
Tubulin
Contractile VSMC
EC
94
68
43
35
23
130
55
Ctrl
Ctrl+oxLDL
DKO
DKO+oxLDL
Fold change
P=0.0063
P=0.0048
P=0.7255
P=0.0018
P=0.0401
P=0.6019
P=0.0265
P=0.0243
P=0.1823
P=0.021
P=0.0312
P=0.1473
P=0.0481
P=0.4990
P=0.7863
P=0.0506
P=0.0003
P=0.10162
D
αSMA
CD31
DAPI
Merge
NRP1
ApoE-/-
VSMC-iDKO/ApoE-/-
50 μm
E
DiI-ac-LDL
DAPI
Merge
100 μm
20 μm
P<0.0001
Cells with DiI (% of cells per view)
ApoE-/-
VSMC-iDKO /ApoE-/-

Supplemental Fig 5. Epsins-specific Deletion Promoted VSMC Differentiating into EC Functional Cells.

A, Quantitation of Dil-Ac-LDL uptake, EC markers CD31 and VE-Cadherin expressions in sorted YFP-tagged cells (n=5).

B, Dil-Ac-LDL uptake assays followed by immuno-staining of VE-Cadherin in sorted YFP-tagged cells. Scale bar=100 μm.

C, VSMC and EC marker genes and protein expressions were measured in long term cultured primary VSMCs isolated from *ApoE*$^{-/-}$ and VSMC-iDKO/*ApoE*$^{-/-}$ mice after treatment with oxLDL (100 μg/ml) for 48 hrs in serum-free media. Quantitation of data (n=5-6).

D, Immuno-staining of EC markers CD31/NRP1 and αSMA in long term cultured VSMC isolated from *ApoE*$^{-/-}$ and VSMC-iDKO/*ApoE*$^{-/-}$ mice with or without the treatment of 100 μg/ml oxLDL for 48 hrs. Scale bar=50 μm.

E, Dil-Ac-LDL uptake in cultured primary VSMCs. Scale bar=100 and 20 μm, respectively. Quantitation of data (n=5).

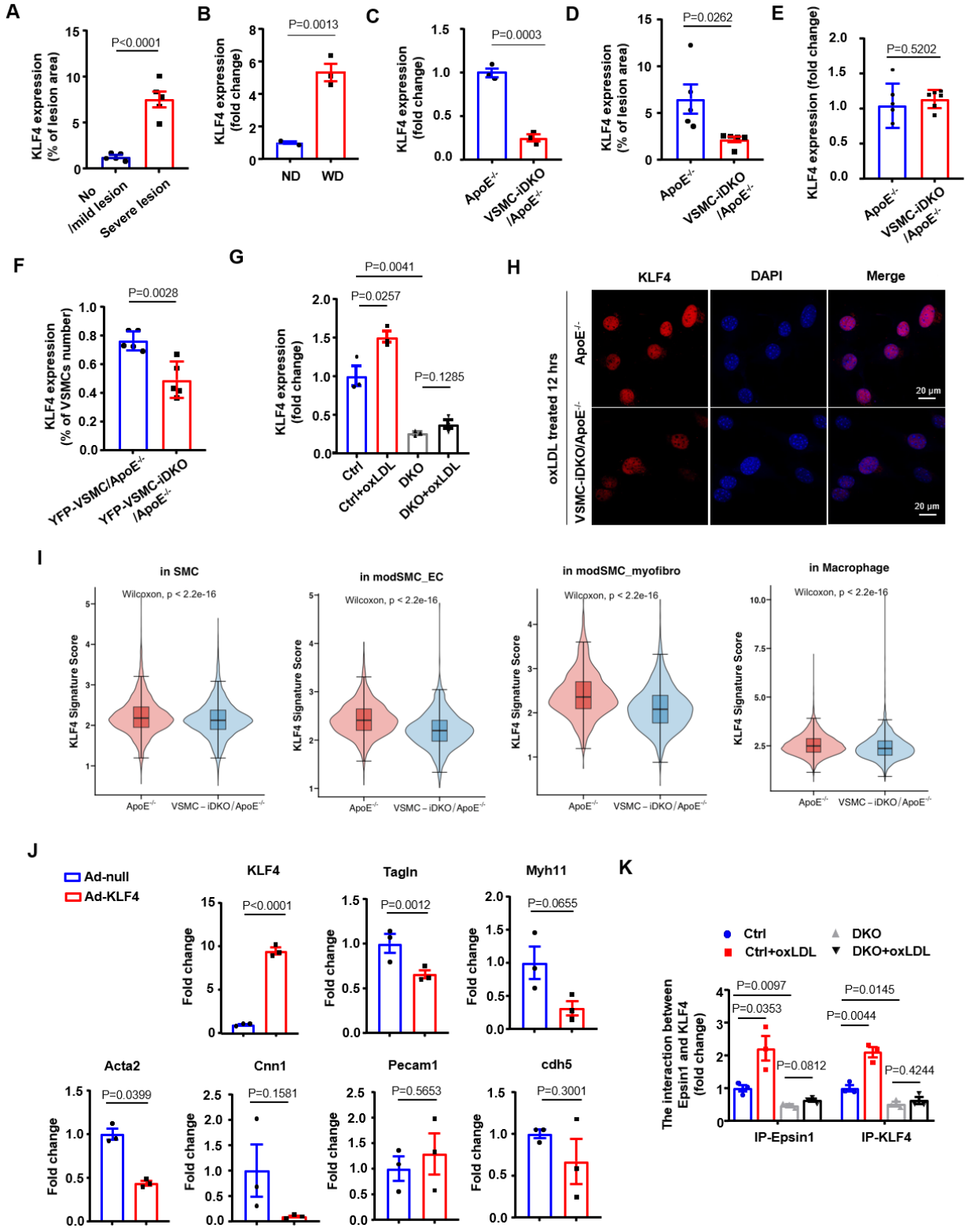
A
KLF4 expression (% of lesion area)
P<0.0001
No /mild lesion
Severe lesion
B
KLF4 expression (fold change)
P=0.0013
ND
WD
C
KLF4 expression (fold change)
P=0.0003
ApoE-/-
VSMC-iDKO /ApoE-/-
D
KLF4 expression (% of lesion area)
P=0.0262
ApoE-/-
VSMC-iDKO /ApoE-/-
E
KLF4 expression (fold change)
P=0.5202
ApoE-/-
VSMC-iDKO /ApoE-/-
F
KLF4 expression (% of VSMCs number)
P=0.0028
YFP-VSMC/ApoE-/-
YFP-VSMC-iDKO /ApoE-/-
G
KLF4 expression (fold change)
P=0.0041
P=0.0257
P=0.1285
Ctrl
Ctrl+oxLDL
DKO
DKO+oxLDL
H
KLF4
DAPI
Merge
oxLDL treated 12 hrs
ApoE-/-
VSMC-iDKO/ApoE-/-
20 μm
I
in SMC
in modSMC_EC
in modSMC_myofibro
in Macrophage
Wilcoxon, p < 2.2e-16
KLF4 Signature Score
ApoE-/-
VSMC – iDKO / ApoE-/-
J
Ad-null
Ad-KLF4
KLF4
Tagln
Myh11
Acta2
Cnn1
Pecam1
cdh5
Fold change
P<0.0001
P=0.0012
P=0.0655
P=0.0399
P=0.1581
P=0.5653
P=0.3001
K
Ctrl
Ctrl+oxLDL
DKO
DKO+oxLDL
The interaction between Epsin1 and KLF4 (fold change)
P=0.0097
P=0.0353
P=0.0812
P=0.0145
P=0.0044
P=0.4244
IP-Epsin1
IP-KLF4

Supplemental Fig 6. Epsins Suppressed the Expression of VSMC markers by Decreasing KLF4 Expression

A, Quantitation of KLF4 expression in human samples (n=3).

B-C, Quantitation of western blot analysis of KLF4 expression (n=3).

D, Quantitation of KLF4 expression in truncus brachiocephalicus of SMC-lineage tracing mice fed a WD for 20 weeks (n=5).

E, The mRNA expression of KLF4 in aortas from ApoE$^{-/-}$ and VSMC-iDKO/ApoE$^{-/-}$ mice fed a WD for 20 weeks (n=6).

F, Quantitation of KLF4 expression in sorted YFP-tagged cells (n=6).

G, Quantitation of western blot analysis of KLF4 expression (n=3).

H, Immuno-staining of KLF4 in primary VSMCs isolated from ApoE$^{-/-}$ and VSMC-iDKO/ApoE$^{-/-}$ mice with the treatment of 100 μg/ml oxLDL for 12 hrs. Scale bar=20 μm.

I, Differential signature score of KLF4 binding genes between ApoE$^{-/-}$ and VSMC-iDKO/ApoE$^{-/-}$ mice across candidate cell types from scRNA-seq data. *P* value was calculated by Wilcoxon rank sum test. The signature score was calculated using differential 1113 target genes of KLF4 binding site with *PercentageFeatureSet* function deposited in *Seurat* package.

J, The mRNA expressions of *KLF4*, VSMC marker genes and EC markers were measured in primary VSMCs from VSMC-iDKO/ApoE$^{-/-}$ mice transfected with Ad-null or Ad-KLF4 for 24 hrs followed with 12 hrs oxLDL treatment (n=3).

K, Quantitation of the interaction between epsins and KLF4 in primary VSMCs tested with immunoprecipitation and western blot (n=3).

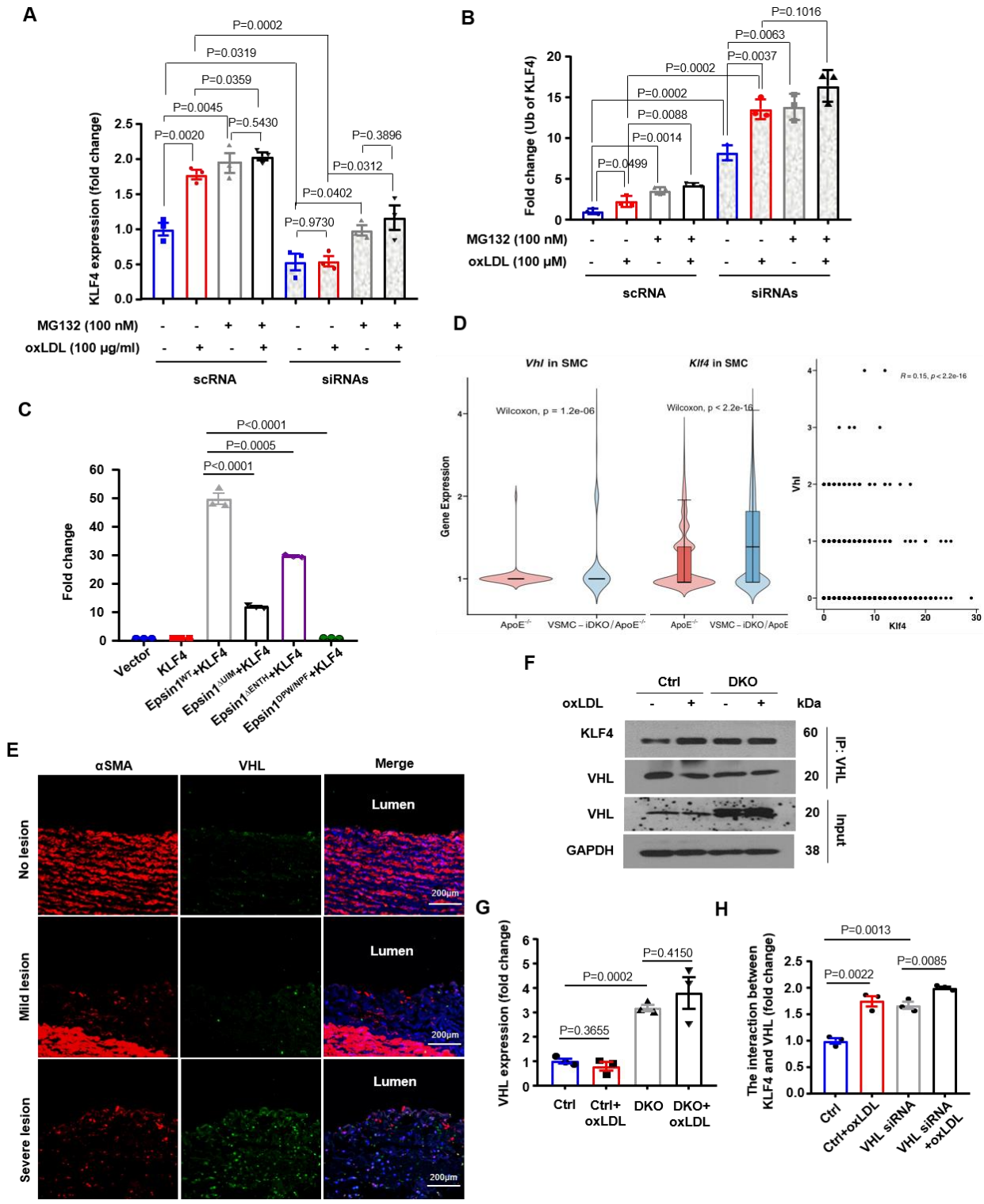
A
KLF4 expression (fold change)
P=0.0002
P=0.0319
P=0.0359
P=0.0045
P=0.5430
P=0.0020
P=0.3896
P=0.0312
P=0.0402
P=0.9730
MG132 (100 nM)
oxLDL (100 μg/ml)
scRNA
siRNAs
B
Fold change (Ub of KLF4)
P=0.1016
P=0.0063
P=0.0037
P=0.0002
P=0.0002
P=0.0088
P=0.0014
P=0.0499
MG132 (100 nM)
oxLDL (100 μM)
scRNA
siRNAs
C
Fold change
P<0.0001
P=0.0005
P<0.0001
Vector
KLF4
Epsin1WT+KLF4
Epsin1ΔUIM+KLF4
Epsin1ΔENTH+KLF4
Epsin1DPW/NPF+KLF4
D
Vhl in SMC
Klf4 in SMC
Wilcoxon, p = 1.2e-06
Wilcoxon, p < 2.2e-16
Gene Expression
ApoE-/-
VSMC – iDKO/ApoE-/-
R = 0.15, p < 2.2e-16
Vhl
Klf4
E
αSMA
VHL
Merge
No lesion
Mild lesion
Severe lesion
Lumen
200μm
F
Ctrl
DKO
oxLDL
kDa
KLF4
VHL
VHL
GAPDH
60
20
20
38
IP: VHL
Input
G
VHL expression (fold change)
P=0.4150
P=0.0002
P=0.3655
Ctrl
Ctrl+ oxLDL
DKO
DKO+ oxLDL
H
The interaction between KLF4 and VHL (fold change)
P=0.0013
P=0.0022
P=0.0085
Ctrl
Ctrl+oxLDL
VHL siRNA
VHL siRNA +oxLDL

Supplemental Fig 7. Epsins hindered KLF4 ubiquitination via preventing VHL binding to KLF4.

A-B, Quantitation of western blot analysis of KLF4 expression and ubiquitination (n=3).

C, Quantitation of the interaction between epsin 1 or epsin 1 domains and KLF4 in HEK293 cells (n=3).

D, Differential gene expression and correlation of *Vhl* and *Klf4* between ApoE$^{-/-}$ and VSMC-iDKO/ApoE$^{-/-}$ mice in SMC cells derived from scRNA-seq data. *P* value was calculated by Wilcoxon rank sum test and Spearman correlation analysis.

E, Immuno-staining of αSMA, VHL and nuclei in human samples with no, mild or severe atherosclerotic lesion. Scale bar=100 μm.

F-H, Immunoprecipitation of VHL and KLF4 with anti-VHL antibody in primary VSMC isolated from ApoE$^{-/-}$ and VSMC-iDKO/ApoE$^{-/-}$ mice with or without oxLDL treatment (100 μg/ml) and analyzed with western blot (n=3).

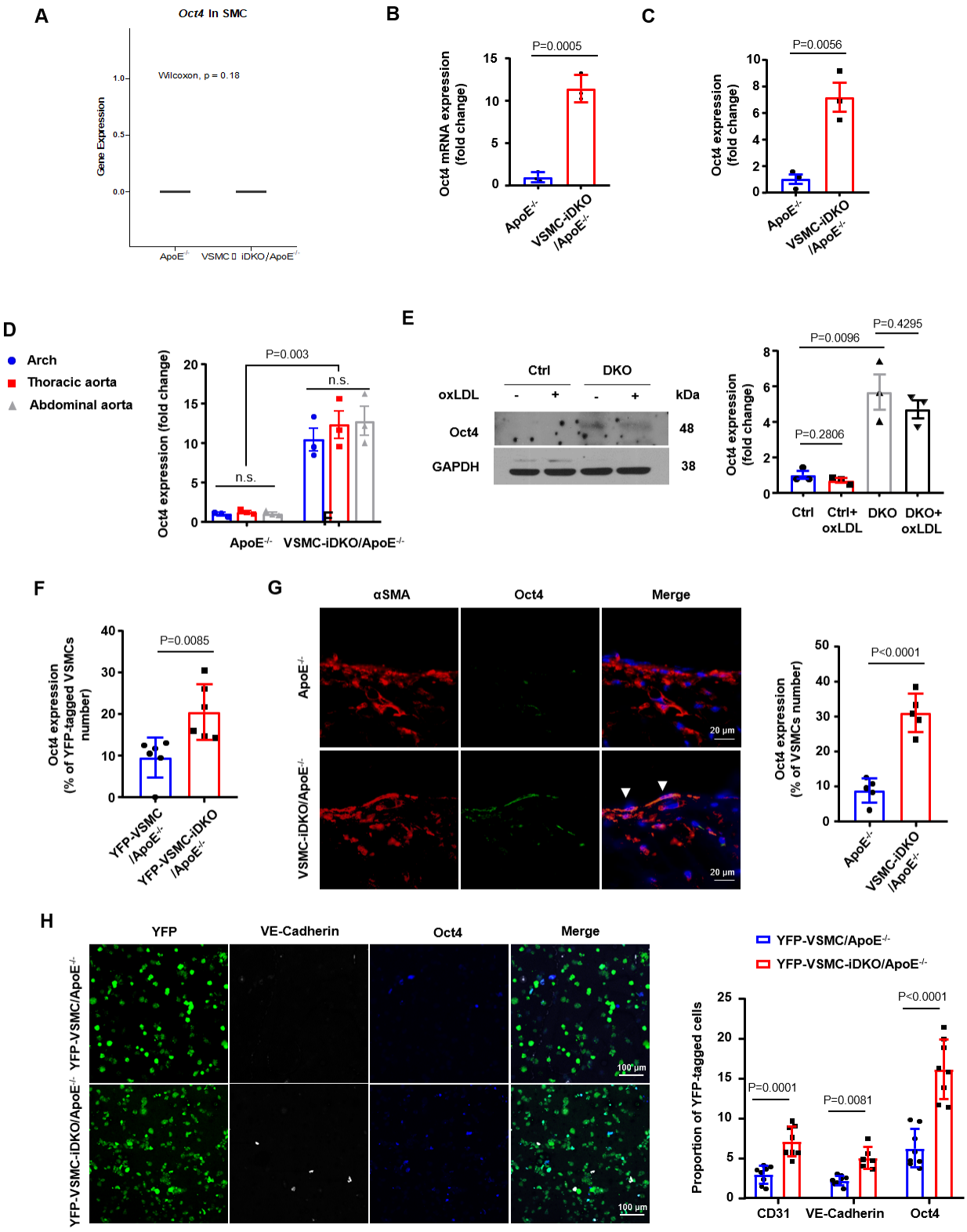
A
Oct4 in SMC
Wilcoxon, p = 0.18
Gene Expression
1.0
0.5
0.0
ApoE-/-
VSMC-iDKO/ApoE-/-
B
P=0.0005
Oct4 mRNA expression (fold change)
15
10
5
0
ApoE-/-
VSMC-iDKO /ApoE-/-
C
P=0.0056
Oct4 expression (fold change)
10
8
6
4
2
0
ApoE-/-
VSMC-iDKO /ApoE-/-
D
Arch
Thoracic aorta
Abdominal aorta
P=0.003
n.s.
n.s.
Oct4 expression (fold change)
20
15
10
5
0
ApoE-/-
VSMC-iDKO/ApoE-/-
E
Ctrl
DKO
oxLDL
-
+
-
+
kDa
Oct4
48
GAPDH
38
P=0.0096
P=0.4295
P=0.2806
Oct4 expression (fold change)
8
6
4
2
0
Ctrl
Ctrl+ oxLDL
DKO
DKO+ oxLDL
F
P=0.0085
Oct4 expression (% of YFP-tagged VSMCs number)
40
30
20
10
0
YFP-VSMC /ApoE-/-
YFP-VSMC-iDKO /ApoE-/-
G
αSMA
Oct4
Merge
ApoE-/-
VSMC-iDKO/ApoE-/-
20 μm
20 μm
P<0.0001
Oct4 expression (% of VSMCs number)
50
40
30
20
10
0
ApoE-/-
VSMC-iDKO /ApoE-/-
H
YFP
VE-Cadherin
Oct4
Merge
YFP-VSMC/ApoE-/-
YFP-VSMC-iDKO/ApoE-/-
100 μm
100 μm
YFP-VSMC/ApoE-/-
YFP-VSMC-iDKO/ApoE-/-
P<0.0001
P=0.0001
P=0.0081
Proportion of YFP-tagged cells
25
20
15
10
5
0
CD31
VE-Cadherin
Oct4

Supplemental Fig 8. VSMC-specific Epsins Deficiency Augmented the Oct4 Expression in Atherosclerotic Plaques

A, Differential gene expression of *Oct4* between ApoE$^{-/-}$ and VSMC-iDKO/ApoE$^{-/-}$ mice in SMC cells derived from scRNA-seq data. *P* value was calculated by Wilcoxon rank sum test.

B, Oct4 mRNA expression in aortas of ApoE$^{-/-}$ and VSMC-iDKO/ApoE$^{-/-}$ mice fed a WD for 20 weeks (n=3). **C-D,** Quantitation of western blot analysis of Oct4 expression in the whole aortas and different part of aortas (n=3).

E, Immuno blot analysis of Oct4 in primary VSMC isolated from ApoE$^{-/-}$ and VSMC-iDKO/ApoE$^{-/-}$ mice with or without the treatment of 100 μg/ml oxLDL for 24 hrs (n=3).

F, Quantitation of Oct4 expression in sorted YFP-tagged cells (n=5-6).

G, Immuno-staining of αSMA and Oct4 in aortic roots of ApoE$^{-/-}$ and VSMC-iDKO/ApoE$^{-/-}$ mice fed a WD for 20 weeks. Scale bar=20 μm. Quantitation of data (n=5).

H, The localization of Oct4 and VE-Cadherin expression in sorted YFP-tagged cells under confocal microscope. Scale bar=100 μm. Quantitation of data (n=7).

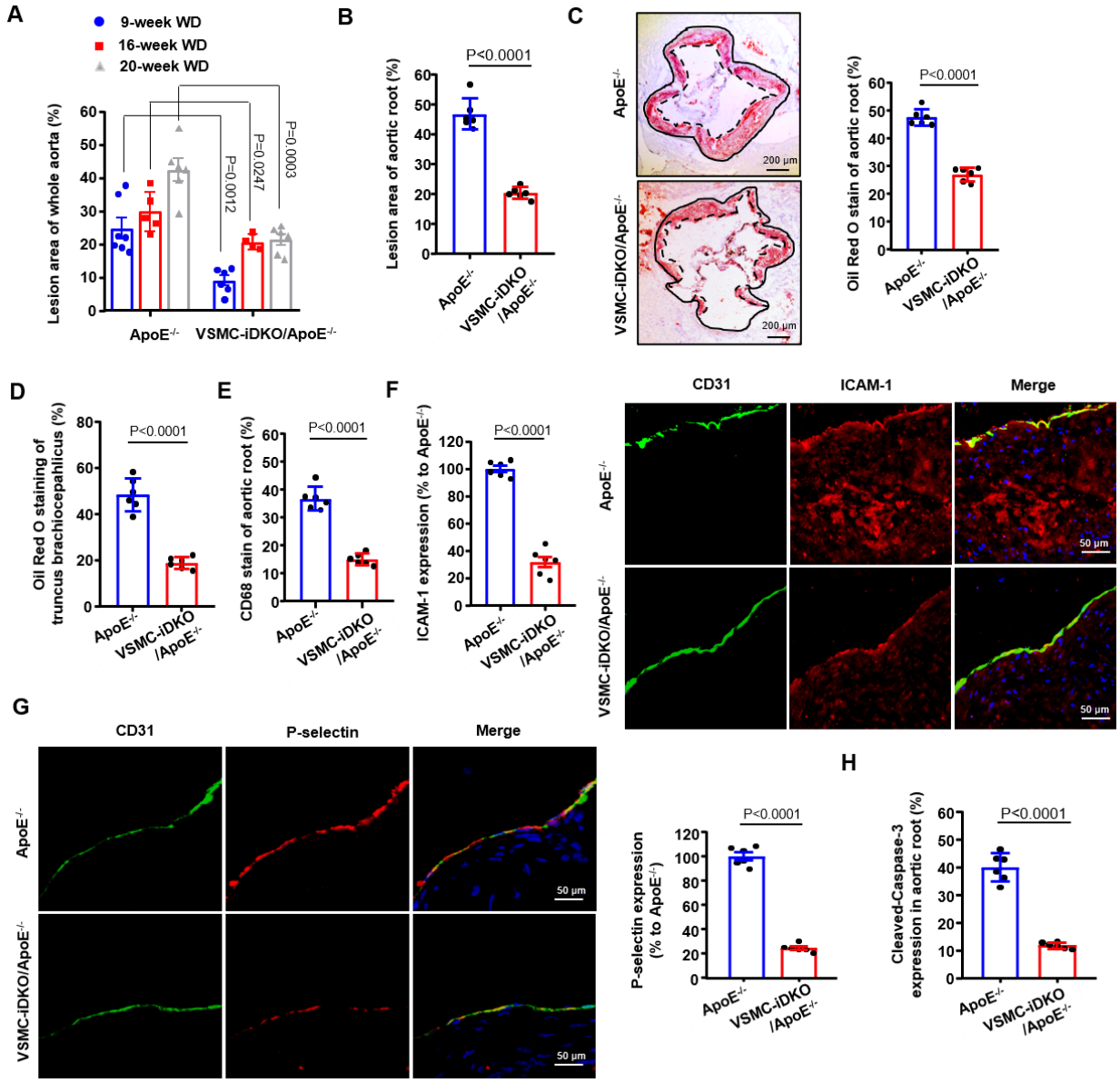
A
9-week WD
16-week WD
20-week WD
Lesion area of whole aorta (%)
P=0.0012
P=0.0247
P=0.0003
ApoE-/-
VSMC-iDKO/ApoE-/-
B
P<0.0001
Lesion area of aortic root (%)
ApoE-/-
VSMC-iDKO /ApoE-/-
C
ApoE-/-
VSMC-iDKO/ApoE-/-
200 μm
P<0.0001
Oil Red O stain of aortic root (%)
D
P<0.0001
Oil Red O staining of truncus brachiocepahlicus (%)
E
P<0.0001
CD68 stain of aortic root (%)
F
P<0.0001
ICAM-1 expression (% to ApoE-/-)
CD31
ICAM-1
Merge
50 μm
G
CD31
P-selectin
Merge
50 μm
H
P<0.0001
P-selectin expression (% to ApoE-/-)
P<0.0001
Cleaved-Caspase-3 expression in aortic root (%)

Supplemental Fig 9. VSMC-specific Epsin 1 and 2 Deficiency reduces the lesion size and inflammation in atherosclerotic plaques.

A-B, Quantitation of lesion area in whole aorta (**A**) and aortic root (**B**) (n=4-7).

C, ORO staining of aortic roots in ApoE$^{-/-}$ and VSMC-iDKO/ApoE$^{-/-}$ mice fed a WD for 20 weeks. Quantitation of data (n=6). Scale bar=200 μm. (n=6).

D, Quantitation of lesion area in truncus brachiocephalicus (n=6).

E, Quantitation of CD68 expression in the lesion of aortic root (n=6).

F-G, Immuno-staining of CD31 and ICAM-1 (**F**) or P-selectin (**G**) in dissected aortic roots from ApoE$^{-/-}$ or VSMC-iDKO/ApoE$^{-/-}$ mice fed a WD for 20 weeks. Scale bar=50 μm. Quantitation of data (n=6).

H, Quantitation of cleaved-caspase3 expression in the lesion of aortic root (n=6).

Antibodies used in this study

Antibody	Sources	Cat#	Source/ Isotype	Applications	Cross activity	MW (kDa)
KLF4	Abcam	ab129473	Rabbit	WB, ICC/IF	H M	60
Oct4	Abcam	ab200834	Rabbit	WB, IHC-P, ICC/IF, IP, F	H M	45
VHL	Cell signaling	68547S	Rabbit	WB	H	18~22
Cleaved-capase3	Cell signaling	9661	Rabbit	WB, IHC, IF, IP, F	H M R Mk	17 19
NRP1	Abcam	ab81321	Rabbit	WB, IHC-P, ICC/IF, IP, F	H M R	103
Galectin3	Abcam	ab2785	MS	WB, ICC/IF, IHC-P	H M	26
Ecrg4	Abcam	ab224077	MS	WB, IHC-P	H	17
α-SMA-cy3	Sigma	C6198-.2ml	MS	IF	H M	
VE-Cadherin	R&D	AF1002	Goat	WB, IHC	M	
MYH11	Abcam	ab224804	Rabbit	IF, WB	M R H	42
SM22 (Tagln)	Abcam	ab14106	Rabbit	ICC/IF, WB	M R H	23
Calponin 1	Abcam	ab46794	Rabbit	WB, IHC-P, ICC/IF	M R H P	34
CD31	BD Pharmingen	550274	Rat	IF	M H R	
CD68	Santa Cruz	sc-20060	MS	IF	M H	
Epsin 1	Home made	n/a	Rabbit	WB, IP, IF	H M	75~80
Epsin 2	Home made	n/a	Rabbit	WB, IP, IF	H M	65~70
HA.11	BioLegend	901502	MS	WB, IP	all	n/a
ICAM-1	Santa Cruz	sc-8419	MS	WB, IP, IF, IHC(P), F	M H R	
P-selectin	Santa Cruz	sc-271267	MS	WB, IP, IF, ELISA, F	M H R	
ß-actin	Cell signaling	4967	Rabbit	WB	H M R, etc	45
GAPDH	Santa Cruz	Sc-166545	MS	WB	H M	37-43

Secondary antibodies (Invitrogen)

Alexa Fluor 488 (Green)	Alexa Fluor 594 (Red)	Alexa Fluor 647 (Blue)
Donkey anti-Mouse (A21202)	Donkey anti-Mouse (A23744)	Donkey anti-Mouse (A31571)
Donkey anti-Rabbit (A21206)	Donkey anti-Rabbit (A21207)	Donkey anti-Rabbit (A31573)
Donkey anti-Rat (A21208)	Donkey anti-Rat (A21209)	Goat anti-Rat (A21247)
Donkey anti-Goat (A11055)	Donkey anti-Goat (A11058)	

Table S1: Primers used in the RT-PCR for mouse EndoMT marker genes

Mouse genes	Primers
KLF4	KLF4_L1 5'-GATCTCGGGCAATCTGGGG-3' KLF4_R1 5'- TTCCTCACGCCAACGGTTAGT-3'
VE-Cadherin	VE-Cadherin_L1 5'-TACCACTTCAAGCTGCCAGA-3' VE-Cadherin_R1 5'-TCGGAAGAATTGGCCTCTGT-3'
PECAM-1 (CD31)	PECAM-1_L1 5'-GGTCGTGAATGACACCCAAG-3' PECAM-1_R1 5'-ACTCTGACTGCAAGAGTGCT-3'
Oct4	Oct4_L1 5'-AAGTTGGCGTGGAGACTTT-3' Oct4_R1 5'-TTCCACCTTCTCCAACTTCAC-3'
Acta2 (α-SMA)	Acta2_L1 5'-GTCCCTCTATGCCTCTGGAC-3' Acta2_R1 5'-AAGGAATAGCCACGCTCAGT-3'
Myh11	Myh11_L1 5'- CTCTGGCCTCTTCTGTGTGG-3' Myh11_R1 5'-TTTCCAGCTCCCCCGTGAT-3'
Cnn1	Cnn1_L1 5'-CTGTTGCGCTTGTCTGTGTC-3' Cnn1_R1 5'-TGCAGCTTGTTGATAAATTCGC-3'
Tagln	Tagln_L1 5'-GTGAGCCAAGCAGACTTCCAT-3' Tagln_R1 5'-CCAATTTGCTCAGAATCACACC-3'
Lgals3	Lgals3_L1 5'-CTAATCAGGAAAATGGCAGACAG-3' Lgals3_R1 5'-TCCTTGAGGGTTTGGGTTTC-3'
Ecrg4	Ecrg4_L1 5'-AGATGCTCCAGAAACGAGAAG-3' Ecrg4_R1 5'-TCCTTTGCTGTGTTCTCGG-3'